Development of surface-enhanced Raman scattering-based assays with bioorthogonal Raman reporters for quantification of nucleic acids

Ryo Ota

2021

Kyoto Institute of Technology

Contents

General Introduction

Recently, liquid biopsies are used in the detection of next-generation diagnostic biomarkers, such as circulating tumor cells (CTC), cell-free nucleic acids (cfDNAs and cfRNAs), and extracellular vesicles (exosomes and apoptotic bodies), in body fluids, such as blood, saliva, urine and stool from patients (**Figure 1**) [1–3]. Conventional tissue biopsies are surgical procedures in which a small amount of tumor tissues is removed for the diagnosis. On the other hands, liquid biopsies are minimally invasive diagnostic techniques that allow for early diagnosis, staging, prognosis and follow-up. Particularly, the detection methods of cell-free nucleic acids are expected as a novel diagnostic method that enables early diagnosis of serious diseases such as cancer [4] and viral diseases [5]. Quantification polymerase chain reaction (qPCR) is the gold standard among conventional nucleic acid detection methods and is used for highly sensitive quantifying nucleic acids [6]. However, since qPCR requires the purification of samples and the time-consuming process for enzymatic amplification of nucleic acids, it is not generally used as a diagnostic method. Recently, surface-enhanced Raman scattering (SERS), which is also used for the single-molecule detection, is expected as a promising method for detecting nucleic acids without the amplification process [7]. The aim of this study is the development of novel SERS-based assays for a simple and accurate detection of nucleic acids using bioorthogonal Raman reporters.

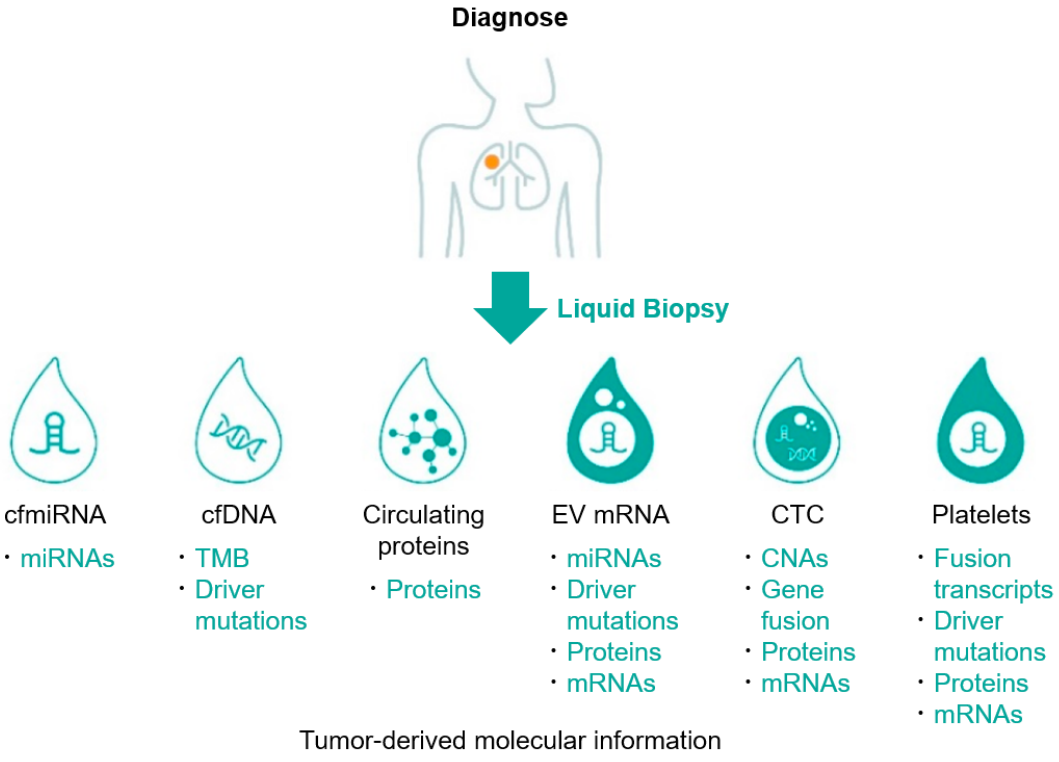

Figure 1. Circulating biomarkers for diagnosis, prediction, and monitoring response to therapy in several diseases by liquid biopsy.

Nucleic acid detection methods

Nucleic acid detection methods have an essential role in the diagnosis of serious diseases such as cancer and viral diseases [4,5]. Here, I describe the conventional methods for detection of nucleic acids.

Quantitative polymerase chain reaction

PCR is an amplification method to produce numerous copies of target DNAs by using forward and reverse primers and DNA polymerases [8]. In the case of detecting RNAs, cDNA is amplified by PCR after reverse transcription of RNA of interest. Conventional PCR-based methods analyze PCR amplicons at the end of the reaction using gel visualization and sequencing [9].

qPCR is a highly sensitive method for quantifying nucleic acids of interest in real-time [6]. In qPCR, fluorescence probes such as EtBr [10], SYBR Green [11], and TaqMan probe [12] are used for monitoring the amplicons (**Figure 2**). The starting copy number of the target nucleic acids is estimated from the PCR cycle threshold value (Ct value). This technique is widely used for sensitively and selectively quantifying the nucleic acids in laboratory and clinical fields.

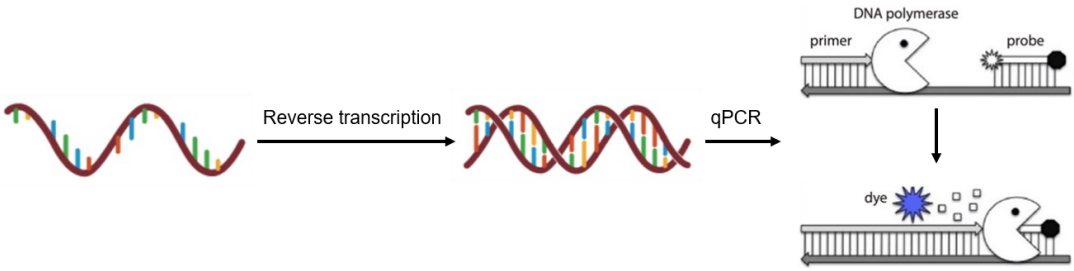

Figure 2. Schematic diagram of the procedure for the qPCR with TaqMan probes.

Microarray

Microarray is ideally suited for high-throughput screening of RNA because a single microchip allows to coincidentally analyze hundreds of RNA sequences [13,14]. In the most basic method, the RNA sample extracted from a biological specimen is first treated with a reverse transcription and a fluorescent tagging process (**Figure 3**). Then, fluorescent-labeled cDNAs are hybridized with DNA probes immobilized on a microchip. After washing process, the fluorescent-labeled cDNAs are quantified from fluorescence signals observed on the microchip.

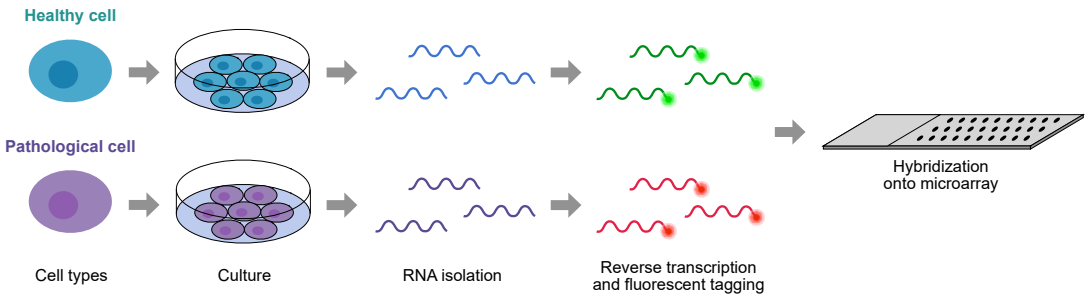

Figure 3. Procedure for the detection of RNAs by the DNA microarray.

Loop mediated isothermal amplification

Isothermal nucleic acid amplification (LAMP) is a novel isothermal nucleic acid amplification method (Optimum temperature: 60–65 °C) [15]. The LAMP uses six types of primers (forward outer primer: F3, backward outer primer: B3, forward inner primer: FIP, backward inner primer: BIP, forward loop primer: Loop F, backward loop primer: Loop B) and a DNA polymerase with strand-displacement activity (**Figure 4**). First, upon hybridization of FIP with the target DNA, FIP-linked complementary strand is synthesized by DNA polymerase. Then, elongation of F3 leads to displacement of the FIP-linked complementary DNA, releasing single strand DNA (ssDNA) as a template of the backward primers. BIP starts synthesis of complementary strands at the ssDNA and then displacement of BIP-linked complementary strands occurs in association with elongation of B3. Both the 3'- and 5'-end of synthesized stands are complementary to sequences further inwards, forming a stem-loop configuration (a dumbbell-like strand). Formation of hairpin structure induces elongation of its 3'-end (F1) and displacement of the 5'-end (B1c), generating the new hairpin strand at 3'-end. Reiteration of the elongation of dumbbell-like strands generates long amplicons. Additionally, inner and outer primers hybridize with the loop parts (F2c, B2c) and start strand synthesis and displacement. Loop primers, which hybridize with the loop parts, accelerate amplification reaction. LAMP amplicons are detected by gel electrophoresis [16], precipitation of magnesium pyrophosphate [17], and fluorescent dye [18]. Particularly, in the LAMP-based detection methods using magnesium pyrophosphate and fluorescent dye, monitoring the haze of the pyrophosphate and the fluorescence of dye enables the real-time detection of amplicons [19,20].

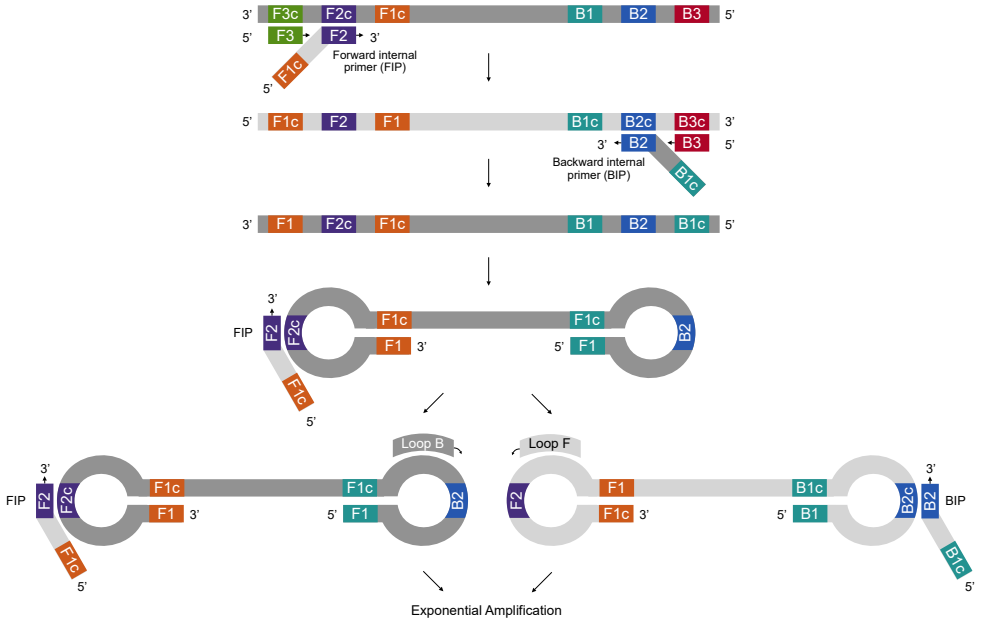

Figure 4. Schematic diagram of the procedure for the LAMP.

Surface-enhanced Raman scattering

In 1928, Raman *et al*. discovered the inelastic Raman scattering that provides the unique information about the vibrational and rotational energies of molecular bonds [21]. The fingerprint features of Raman scattering allow for the molecular diagnosis. However, Raman scattering is an inherently weak scattering with only one in 10^6 photons being scattered so that Raman spectroscopy is hardly used for detection of molecules of interest. In 1970s, it was reported that the Raman scattering of the sub-monolayer coverages of molecules surfaces is significantly enhanced on roughened coinage metal [22,23]. Thereafter, this phenomenon was defined as SERS and has been researched and applied for detection of biological molecules, from small molecules such as glucose [24,25] and amino acids [26,27] to large molecules such as DNA [28,29], RNA [30,31], proteins [32,33], and lipids [34,35].

Surface-enhanced Raman scattering electromagnetic mechanism [36,37]

SERS is a vibrational spectroscopic technique that amplifies the Raman scattering of the molecules adsorbed on the metal nanostructure by 10^8– to 10^{10}–fold [38]. The SERS enhancement arises from two mechanisms: (1) an electromagnetic enhancement and (2) a chemical enhancement such as a resonance Raman scattering [39]. Of these mechanisms, the electromagnetic enhancement largely contributes to the SERS enhancement. Here, I mainly describe the electromagnetic enhancement mechanism.

1. Localized surface plasmon resonance

The localized surface plasmon resonance (LSPR) is induced when the collective oscillation of free electrons of a metal nanoparticle is in resonance with the incident light (**Figure 5**). The LSPR-induced electromagnetic field enhances the Raman signals of the molecules adsorbed on the metal nanoparticles. In the case of spherical nanoparticles, the magnitude of the electromagnetic field outside the particles, E_{out}, is given by

$$E_{out}(x,y,z) = E_{in}\hat{\boldsymbol{z}} - \alpha E_{in}\left(\frac{\hat{\boldsymbol{z}}}{r^3} - \frac{3z}{r^5}(x\hat{\boldsymbol{x}} + y\hat{\boldsymbol{y}} + z\hat{\boldsymbol{z}})\right), \quad (1)$$

where E_{in} is the magnitude of the incident field; x, y, and z are the Cartesian coordinates; $\hat{\boldsymbol{x}}$, $\hat{\boldsymbol{y}}$, and $\hat{\boldsymbol{z}}$ are the Cartesian unit vectors; r is the radial distance; and α is the metal polarizability expressed as

$$\alpha = a^3 \frac{\varepsilon_m(\omega) - \varepsilon_d}{\varepsilon_m(\omega) + 2\varepsilon_d}, \quad (2)$$

where a is the radius of the sphere; ω is the angular frequency; ε_m is the dielectric constant of metal nanoparticle; and ε_d is the dielectric constant of the external environment [40,41]. **Equation 1** shows that the field enhancement increases in proportion to r^{-3}. The maximum enhancement occurs when the denominator of α approaches zero ($\mathrm{Re}[\varepsilon_m] \approx -2\varepsilon_d$). Furthermore, another important parameter for plasmon resonance is a quality factor Q defined as [36,42]

$$Q = \frac{\omega \frac{d}{d\omega}\mathrm{Re}[\varepsilon_m]}{2(\mathrm{Im}[\varepsilon_m])^2}. \quad (3)$$

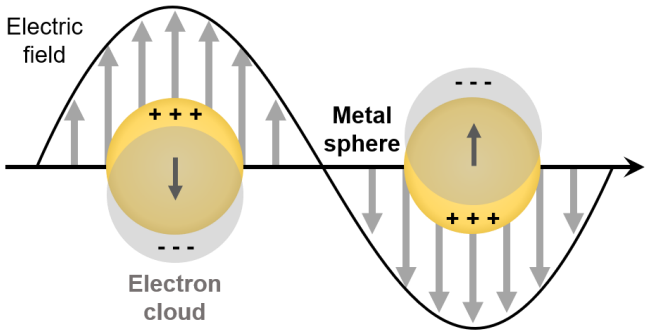

Figure 5. Illustration of the localozed surface plasmon resonance effect.

The higher Q factor, which represents a sharper resonance, is often desirable as it leads to stronger local-field enhancement. **Equation 3** shows that the Q factor is dependent on only the dielectric constant of metal nanoparticles at the frequency, not on the shape of metal nanoparticles. Namely, to obtain a stronger local-field enhancement, it is important to choose the metal material and resonance frequency.

From these qualitative arguments, one can considered that metals that meet the following conditions are suitable for plasmonics:

- $\mathrm{Re}[\varepsilon_m]$ is negative in the wavelength range of the visible and near infrared (400–1000 nm). As a rule of thumb, it is desirable that $\mathrm{Re}[\varepsilon_m]$ is in a range from -20 to -1 for LSPR-based applications.
- $\mathrm{Im}[\varepsilon_m]$ is small or Q factor is large in the wavelength of interest. Practically, Q should be larger than 2, preferably larger than 10.

From the examples of various metal, silver, gold, and copper are suitable for plasmonics at longer wavelength (400–1000 nm) and are widely used for SERS and plasmonic applications. Notably, silver is the material of choice for localized surface plasmonic field enhancement using the incident light below ~600 nm. Considering the practical issues (availability, ease of manipulation, especially for the fabrication of nanostructures, toxicity, durability, cost, etc.), gold is the most promising material and is often used for the plasmonics using the incident light beyond ~600 nm.

2. E^4 enhancement

SERS occurs only when a molecule is near the surface of the metal nanostructure (**Figure 6**). The adsorbed molecule interacts with local electric field $E_{in}(\omega_{in})$ generated by exciting metal nanoparticles with incident laser. The induced Raman scattering with ω_{in}–ω_{vib}, where ω_{vib} is angular eigenfrequency of vibrating molecule, also excites a LSPR of the metal nanostructure and generates the electromagnetic field $E(\omega_{in}$–$\omega_{vib})$. The SERS intensity is dependent on both the incoming angular frequency ω_{in} and the outcoming angular frequency ω_{in}–ω_{vib}, and it is described as

$$I_{SERS} = I_{in}(\omega_{in})I(\omega_{in} - \omega_{vib}) = |E_{in}(\omega_{in})|^2|E(\omega_{in} - \omega_{vib})|^2. \quad (4)$$

In Raman scattering, because ω_{in}–ω_{vib} approximately corresponds to ω_{in} (ω_{in}≈ω_{in}–ω_{vib} or $\omega_{in} \gg \omega_{vib}$), the SERS intensity is approximated as $I_{SERS} \approx |E_{in}(\omega_{in})|^4$ [43].

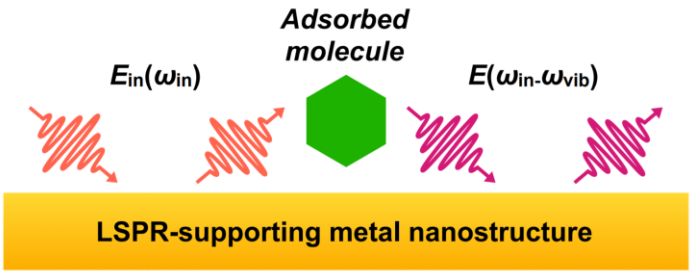

Figure 6. Illustration of electromagnetic enhancement mechanism in SERS.

3. Distance Dependence

In SERS, the distance between a molecule and a surface of metal nanoparticles is critical factor. The strength of electromagnetic fields $E(r)$ around small metal nanoparticles scales with $1/r^3$. Using E^4 approximation, the SERS intensity I_{SERS} is proportional to $1/r^{12}$. Considering the increased surface area of metal nanoparticle scaling with r^2, the distance dependence of SERS intensity scales with $1/r^{10}$ and is described as:

$$I_{SERS} = \left(\frac{a+r}{a}\right)^{-10}, \quad (5)$$

where a is the average size of the field-enhancing features on the surface; and r is the distance from the surface to the adsorbed molecule [44,45].

4. Shape and LSPR wavelength of SERS substrates

Excitation with the laser suitable for LSPR wavelength is required to obtain great SERS enhancement [45,46]. The LSPR wavelength also depends on the shape and composition of metal nanostructure (e.g., silver nanoparticle: 400–500 nm; gold nanoparticle: 500–600 nm; gold nanorod: 600–1000 nm; gold nanostar: 600–800 nm) [40,47]. Additionally, the SERS enhancement factor is closely related to the shape of metal nanostructures [46]. Although gold nanoparticles are widely used for SERS application, generation of the "hot-spots" through aggregation of nanoparticles is needed for

effectively amplifying the Raman scattering. On the other hands, gold nanorods and nanostars cause the strong SERS enhancement without aggregation in comparison with gold nanoparticles. Especially, gold nanostars show the highest SERS enhancement under the irradiation of laser with suitable wavelength for LSPR [46].

SERS-based assays for detection of nucleic acids

SERS-based assays for detection of nucleic acids have been studied as a novel detection method to replace qPCR and are roughly classified into two types approach: (1) label-free nanoparticles, and (2) labeled nanoparticle (**Figure 7**) [48–50]. Here, I describe the SERS-based assays using the two types approach and their applications.

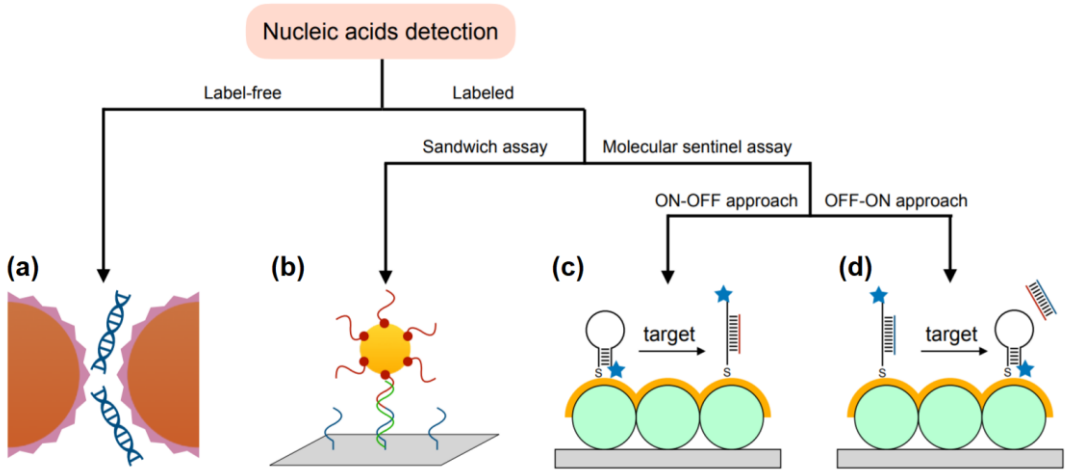

Figure 7. Approaches of SERS-based assays for detection of nucleic acids. (a) Label-free detection method of nucleic acids. (b) Sandwich assay for detection of nucleic acids. Raman reporter-modified hairpin DNA probes for detection of nucleic acids based on (c) ON-OFF approach and (d) OFF-ON approach.

1. Label-free nanoparticles

In label-free nanoparticle-based assays for detection of nucleic acids, nucleic acids are captured by the weak interaction of naked metal nanoparticles and nucleic acids and are detected by its own Raman signals.

In 2008, Halas *et al.* reported that label-free SERS detection of DNA using SiO_2@Au core-shell nanostructure [51]. This report demonstrated that high-quality and reproducible SERS spectra of single-stranded and double-stranded DNA was successfully obtained. In 2014, Graham *et al*. presented positively charged silver nanoparticles coated with spermine molecules for detection of DNA with negatively charged [52]. This work demonstrated that the aggregation of silver nanoparticles was induced by the interaction of a phosphate group of DNAs with spermine, allowing for the improvement reproducibility of SERS spectra and highly sensitive detection of DNA. In 2015, Ren *et al.* reported that iodide-modified silver nanoparticles were used for sensitive and reproducible label-free nanoparticle-based detection of single- and double-DNA [53].

2. Labeled nanoparticles

In labeled nanoparticle-based assays for detection of nucleic acids, oligonucleotides- and Raman reporter-modified metal nanostructures are used for detection of target DNA in a sequence selective manner. Labeled nanoparticle-based assays are done with either sandwich assays or molecular sentinel assays.

2.1. Sandwich assay

In sandwich assay, oligonucleotide-immobilized solid phase and metal nanoparticle labeled with oligonucleotides and Raman reporters are designed to form a sandwich-type complex with target nucleic acids. The SERS signals derived from Raman reporters are obtained in the presence of target nucleic acids.

In 2000, the first report of detection of DNA and RNA using the SERS-based sandwich assay was presented by Mirkin and co-workers [28]. This approach allows for the multiplex DNA detection with a limit of detection (LOD) of 20 fM. In 2008, Irudayaraj *et al.* developed gold nanoparticles labeled with non-fluorescent Raman reporters and DNA probes for the multiple detection of alternative splice junctions of breast cancer susceptibility gene 1 (BRCA1) [54]. In 2012, Wang *et al*. demonstrated that silica-coated silver nanoparticle with Raman reporters for SERS-based sandwich assay were successfully applied to detect target DNAs and exhibited good specificity for the target DNAs [55]. In 2013, silica-coated silver nanorices with Raman reporters and oligonucleotides were developed for detection of the HBV DNA by Wu *et al*. and allows to detect down to 50 aM of HBV DNA [56].

2.2. Molecular sentinel assay

In molecular sentinel assays, metal nanostructures labeled with Raman reporter-functionalized hairpin DNA are used for detection of nucleic acids. These assays are classified into two types: (1) ON-OFF approach, and (2) OFF-ON approach. In the ON-OFF approach, when the hairpin DNA is hybridized with the target DNA, the hairpin DNA changes from a stem-loop configuration to open state, resulting in a decrease in the SERS signal on Raman reporters. The OFF-ON approach is the opposite phenomenon of the ON-OFF approach. In the initial stage, the hairpin DNA forms the open state since the hairpin DNA is hybridized with placeholder. When the target DNA is hybridized with the placeholder, the hairpin DNA changes from the open state to the stem-loop configuration, resulting in an increase in the SERS signal.

Vo-Dinh *et al*. reported for the first time the molecular sentinel assay using silver nanoparticle based on ON-OFF approach for detection of gene sequence of human immunodeficiency virus (HIV) [57] and demonstrated the feasibility of multiplex detection using SERS-based molecular sentinel assay [58]. This group further developed a plasmonic nanowave chip labeled with hairpin DNAs as a rapid and cost-effective biosensor for detection of nucleic acids. In 2013, ON-OFF-based molecular sentinel

assay using the plasmonic nanowave chip was developed for the specific detection of a common inflammation biomarker [29]. Furthermore, in 2015, molecular sentinel assay using the plasmonic nanowave chip based on OFF-ON approach was reported to detect specific DNA of the dengue virus 4 after single reaction on the chip without any washing step [59].

3. Sensitivity of SERS-based assays

The LOD is essential parameters to evaluate the sensitivity of analytical techniques. LODs of the conventional SERS-based assays for detection of the nucleic acids ranged from atto-molar to nano-molar (aM–nM) [48–50]. These LODs are dominated by the following factors: (1) the SERS enhancement capability of the electromagnetic field caused by SERS substrates, (2) the dissociation constant between oligonucleotides-modified SERS substrates and target DNA or RNA, (3) the variation of SERS signals, (4) the sensitivity of instruments, and other factors. Notably, the factor (3) is also related on the reproducibility of SERS-based assays. However, previous reports are focused on only the factor (1) and (2), for example, the development of SERS substrates that can generate a strong electromagnetic enhancement [29,56], and the development of metal nanoparticles modified with locked nucleic acid (LNA) having high affinity to complementary nucleic acids [60,61]. There has been little research of SERS-based assays focused on the factor (3).

Biologically silent region

All mammalian cells exhibit a biologically silent region in which little Raman signal of biomolecules is observed ranging from 1800 to 2800 cm^{-1} [62]. A bioorthogonal Raman reporter, which has a Raman signal in this region, is not interfered by the Raman signals derived from biomolecules and allows to readily discriminate the Raman signal of reporter molecules from that of biomolecules. Raman reporters with an ethynyl group, a nitrile group, a deuterated methylene group, and an azide group were commonly used as the bioorthogonal Raman reporter [63–66]. In particular, the ethynyl group is most promising reporters among the candidates in terms of signal intensity [63]. In 2011, Sodeoka *et al*. demonstrated the first Raman imaging of nuclear localization using 5-ethynyl-2'-deoxyuridine (EdU), which generate a Raman band at 2120 cm^{-1}, in living cells [62]. Recently, SERS-based sensing methods with bioorthogonal Raman reporters for sensitive detection of biomolecules have been developed. In 2019, Liu *et al*. reported that gold nanoparticles modified with alkyne and nitrile groups were developed for multicolor imaging of cancer cells and human breast cancer tissues [67]. In 2020, Tang *et al.* demonstrated *in vivo* SERS imaging and cancer photothermal therapy using bioorthogonal SERS nanotags with a diacetylene group and aptamers for nuclelin and mucin-1 proteins. [68].

Outline of this thesis

qPCR is commonly used to quantify nucleic acids with high sensitivity. However, application of qPCR to the diagnosis of cancer and infectious diseases is limited due to the complicated and time-consuming procedures for enzymatic amplification and DNA or RNA extraction. Therefore, alternative diagnostic methods that do not require the amplification of nucleic acids are required. SERS-based assays are powerful tools as new diagnostic methods for quantifying the nucleic acids without amplification because SER spectroscopy is a sensitive technique, which can be used for the single molecule detection. Bioorthogonal Raman reporters enable to readily discriminate signals of Raman reporter from signals of biosamples because these reporters have a Raman signal in the biological silent region (1800–2800 cm^{-1}). In this thesis, I focused on suppressing the variation of SERS signals and developed novel SERS-based sandwich-type assays for accurately quantifying nucleic acids using bioorthogonal Raman reporter-modified SERS probes.

Chapter 1 concerns the development of a novel sandwich-type assay for simple and facile detection of nucleic acids using SERS probes composed on a gold nanorod as a SERS substrate and 4-cyano-*N*-(2-mercaptoethyl)benzamide (4CMB), which has a Raman signal in the biological silent region. Investigation of the colloidal stability and hybridization efficiency of SERS probes revealed that SERS probes with 240 strands of oligonucleotides were suitable for the condition of sandwich-type assays. The sandwich-type assay detected target DNA down to 500 pM in a sequence-selective manner.

Chapter 2 concerns the development of a novel ratiometric SERS assay for reliable quantification of nucleic acids using **SERS probe 1** with 3-mercapto-*N*-[4-(2-phenylethynyl)phenyl]propenamide (PEP) as reporter molecules and **SERS probe 2** with *N*-(4-ethynylphenyl)-3-mercaptopropanamide (EP) as internal standard, respectively, to improve the reproducibility of SERS intensities. Normalization of SERS intensities by internal standard leads to suppression of the variation of SERS signals, allowing for automatic quantification of target nucleic acids down to 86 pM.

References

[1]. Cheung, A. H. K.; Chow, C.; To, K. F. *J. Thorac. Dis.* **2018**, *10*, S1645–S1651.

[2]. Neumann, M. H. D.; Bender, S.; Krahn, T.; Schlange, T. *Comput. Struct. Biotechnol. J.* **2018**, *16*, 190–195.

[3]. Zhou, B.; Xu, K.; Zheng, X.; Chen, T.; Wang, J.; Song, Y.; Shao, Y.; Zhen, S. *Signal Transduct. Target. Ther.* **2020**, *5*, 144.

[4]. Zhang, W.; Xia, W.; Lv, Y.; Ni, C.; Yang, L. Cell. Physiol. Biochem. **2017**, *41*, 755–768.

[5]. Fu, Y.; Zhang, Y.; Khoo, B. L. *Med. Res. Rev.* **2021**, *41*, 246–274.

[6]. Navarro, E.; Serrano-Heras, G.; Castaño, M. J.; Solera J. *Clin. Chim. Acta* **2015**, *439*, 231–250.

[7]. Wang, Y.; Irudayaraj, J. *Philos. Trans. R. Soc. B* **2013**, *368*, 20120026.

[8]. Mullis, K.; Faloona, F.; Scharf, S.; Saiki, R.; Horn, G.; Erlich, H. *Cold Spring Harbor Symp. Quant. Biol.* **1986**, *51*, 263–273.

[9]. Higuchi, R.; Dollinger, G.; Waston, R. *Nat. Biotechnol.* **1992**, *10*, 413–417.

[10]. Higuchi, R.; Fockler, C.; Dollinger, G.; Waston, R. *Nat. Biotechnol.* **1993**, *11*, 1026–1039.

[11]. Ririe, K. M.; Rasmussen, R. P.; Wittwer, C. T. *Anal. Biochem.* **1997**, *245*, 154–160.

[12]. Holland, P. M.; Abramson, R. D.; Watson, R.; Gelfand, D. H. *Proc. Natl. Acad. Sci. USA* **1991**, *88*, 7276–7280.

[13]. Schena, M.; Shalon, D.; Davis, R. W.; Brown, P. O. *Science* **1995**, *270*, 467–470.

[14]. Hoheisel, J. D. *Nat. Rev. Genet.* **2006**, *7*, 200–210.

[15]. Notomi, T.; Okayama, H.; Masubuchi, H. *Nucleic Acids Res.* **2000**, *28*, e63.

[16]. Imamoto, T.; Sonobe, T.; Hayashi, K.; *J. Clin. Microbiol.* **2003**, *41*, 2616–2622.

[17]. Tomita, N.; Mori, Y.; Kanda, H.; Notomi, T. *Nat. Protoc.* **2008**, *3*, 877–882.

[18]. Tanner, N. A.; Zhang, Y.; Evans, T. C.; *Biotechniques* **2012**, *53*, 81–89.

[19]. Zhang, X.; Lowe, S. B.; Gooding, J. J. *Biosens. Bioelectron.* **2014**, *61*, 491–499.

[20]. Mayboroda, O.; Katakis, I.; O'Sullivan, C.K. *Anal. Biochem.* **2018**, *545*, 20–30.

[21]. Raman C. V.; Krishnan, K. S. *Nature* **1928**, *121*, 501–502.

[22]. Fleischmann, M.; Hendra, P. J.; McQuillan, A. J. *Chem. Phys. Lett.* **1974**, *26*, 163–166.

[23]. Jeanmaira, D. L.; Van Duyne, R. P. *J. Electroanal. Chem.* **1977**, *84*, 1–20.

[24]. Qi, G.; Jia, K.; Fu, C.; Xu, S.; Xu, W. *J. Opt.* **2015**, *17*, 114020.

[25]. Zhu, J.; Du, H.; Zhang, Q.; Zhao, J.; Weng, G.; Li, J.; Zhao, J. *J. Mater. Chem. C* **2019**, *7*, 3322–3334.

[26]. Negria, P,; Schultz, Z. D. *Analyst*, **2014**, *139*, 5989–5998.

[27]. Satheeshkumar, E.; Karuppaiya, P.; Sivashanmugan, K.; Chao, W.; Tsay, H.; Yoshimura, M.

Spectrochim. Acta A **2017**, *181*, 91–97.

[28]. Cao, Y. C.; Jin, R.; Mirkin, C. A. *Science*, **2002**, *297*, 1536–1540.

[29]. Ngo, H. T.; Wang, H. Fales, A. M. Vo-Dinh, T. *Anal. Chem.* **2013**, *85*, 6378–6383.

[30]. Kadam, U. S.; Schulz, B.; Irudayaraj, J. M. K. *The Plant Journal* **2017**, *90*, 1187–1195.

[31]. Wang, Z.; Zong, S.; Wang, Z.; Wu, L.; Chen, P.; Yun, B.; Cui, Y. *Nanotechnology* **2017**, *28*, 105501.

[32]. Wang, Z.; Yang, H.; Wang, M.; Petti, L.; Jiang, T.; Jia, Z.; Xie, S.; Zhou, J. *Colloids Surf. A Physicochem. Eng. Asp.* **2018**, *546*, 48–58.

[33]. Chang, H.; Kang, H.; Ko, E.; Jun, B. H.; Lee, H. Y.; Jeong, D. H. *ACS Sens.* **2016**, *1*, 645–649.

[34]. Guselnikova, O.; Kalachyova, Y.; Hrobonova, K.; Trusova, M.; Barek, J.; Postnikov, P.; Svorcik, V.; Lyutakov, O. *Sens. Actuators B Chem.* **2018**, *265*, 182–192.

[35]. Bruzas, I.; Lum, W.; Gorunmez, Z.; Sagle, L. *Analyst* **2018**, *143*, 3990–4008.

[36]. Le, R. E. C.; Etchegoin, P. G. *Principles of surface-enhanced Raman spectroscopy: And related plasmonic effects.* Amsterdam, Elsevier, **2009**.

[37]. Stiles, P. L.; Dieringer, J. A.; Shah, N. C.; Van Duyne, R. P. *Annu. Rev. Anal. Chem.* **2008**, *1*, 601–626.

[38]. Campion, A.; Patanjali, K. *Chem. Soc. Rev*. **1998**, *27*, 241–250.

[39]. Moskovits, M.; *J. Raman Spectrosc.* **2005**, *36*, 485–496.

[40]. Kelly, K. L.; Coronado, E.; Zhao, L. L.; Schatz, G. C. *J. Phys. Chem. B* **2003**, *107*, 668–677.

[41]. Yoo, S.; Park, Q. H. *Opt. Express* **2012**, *20*, 16480–16489.

[42]. Wang, F.; Shen, Y. R. *Phys. Rev. Lett.* **2006**, *97*, 206806.

[43]. Le Ru, E. C.; Grand, J.; Félidj, N.; Aubard, J.; Lévi, G.; Hohenau, A.; Krenn, J. R.; Blackie, E.; Etchegoin, P. G. *J. Phys. Chem. C* **2008**, *112*, 8117–8121.

[44]. Kennedy, B. J. Spaeth, S.; Dickey, M.; Carron, K. T. *J. Phys. Chem. B* **1999**, *103*, 3640–3646.

[45]. Dieringer, J. A.; McFarland, A. D.; Shah, N. C.; Stuart, D. A.; Whitney, A. V.; Yonzon, C. R.; Young, M. A.; Zhang, X.; Van Duyne, R. P. *Faraday Discuss.* **2006**, *132*, 9–26.

[46]. Li, M.; Cushing, S. K.; Zhang, J.; Lankford, J.; Aguilar, Z. P.; Ma, D.; Wu, N. *Nanotechnology* **2012**, *23*, 115501.

[47]. Wang, Y.; Yan, B.; Chen, L. *Chem. Rev.* **2013**, *113*, 1391–1428.

[48]. Kahraman, M.; Mullen, E. R.; Korkmaz, A.; Wachsmann-Hogiu, S. *Nanophotonics* **2017**, *6*, 831–852.

[49]. Jamieson, L. E.; Asiala, S. M.; Gracie, K.; Faulds, K.; Graham, D. *Annu. Rev. Anal. Chem.* **2017**, *10*, 415–437.

[50]. Chen, C.; Liu, W.; Tian, S.; Hong, T. *Sensors* **2019**, *19*, 1712.

[51]. Barhoumi, A.; Zhang, D.; Tam, F.; Halas, N. J. *J. Am. Chem. Soc.* **2008**, *130*, 5523–5529.

[52]. Guerrini, L.; Krpetić, Ž.; Van Lierop, D.; Alvarez-Puebla, R. A.; Graham, D. *Angew. Chem. Int. Ed.* **2014**, *54*, 1144–1148.

[53]. Xu, L. J.; Lei, Z. C.; Li, J.; Zong, C.; Yang, C. J.; Ren, B. *J. Am. Chem. Soc.* **2015**, *137,* 5149–5154.

[54]. Sun, L.; Yu, C.; Irudayaraj, J. *Anal. Chem.* **2008**, *80*, 3342–3349.

[55]. Li, J. M.; Wei, C.; Ma, W. F.; An, Q.; Guo, J.; Hu, J.; Wang, C. C. *J. Mater. Chem.* **2012**, *22*, 12100–12106.

[56]. Li, M.; Cushing, S. K.; Liang, H.; Suri, S.; Ma, D.; Wu, N. *Anal. Chem*. **2013**, *85*, 2072–2078.

[57]. Wabuyele, M. B.; Vo-Dinh, T. *Anal. Chem.* **2005**, *77*, 7810–7815.

[58]. Wang, H. N.; Vo-Dinh, T. *Nanotechnology* **2009**, *20*, 065101.

[59]. Ngo, H. T.; Wang, H. N.; Fales, A. M.; Nicholson, B. P.; Woods, C. W.; Vo-Dinh, T. *Analyst* **2014**, *139*, 5655–5659.

[60]. Seferos, D. S.; Giljohann, D. A.; Rosi, N. L.; Mirkin, C. A. *ChemBioChem* **2007**, *8*, 1230–1232.

[61]. Wang, H. N.; Vo-Dinh, T. *Small* **2011**, *7*, 3067–3074.

[62]. Yamakoshi, H.; Dodo, K.; Okada, M.; Ando, J.; Palonpon, A.; Fujita, K.; Kawata, S.; Sodeoka, M. *J. Am. Chem. Soc.* **2011**, *133*, 6102–6105.

[63]. Palonpon, A. F.; Sodeoka, M.; Fujita, K. *Curr. Opin. Chem. Biol.* **2013**, *17*, 708–715.

[64]. Lin, L.; Tian, X.; Hong, S.; Dai, P.; You, Q.; Wang, R.; Feng, L.; Vie, C.; Tian, Z. Q.; Chen, X. *Angew. Chem. Int. Ed.* **2013**, *52*, 7266–7271.

[65]. Hong, S.; Lin, L.; Xiao, M.; Chen, X. *Curr. Opin. Chem. Biol.* **2015**, *24*, 91–96.

[66]. Li, Y.; Wang, Z.; Mu, X.; Ma, A.; Guo, S. *Biotechnol. Adv.* **2017**, *35*, 168–177.

[67]. Li, M.; Wu, J.; Ma, M.; Feng, Z.; Mi, Z.; Rong, P.; Liu, D. *Nanotheranostics* **2019**, *3*,113–119.

[68]. Wang, J.; Liang, D.; Jin, Q.; Feng, J.; Tang, X. *Bioconjugate Chem.* **2020**, *31*, 182–193.

Chapter 1

Sandwich-type detection of nucleic acids by bioorthogonal SERS probes

Abstract: Circulating nucleic acids in body fluids, such as cell-free nucleic acids and viral nucleic acids have received much attention for their great potential as biomarkers in liquid biopsies of serious diseases. Although quantitative polymerase chain reaction (qPCR) has been traditionally used as a laboratory-based assay for measuring nucleic acids, alternative techniques to qualitatively, rapidly, and simply measure the extremely low-abundance nucleic acids are required for the realization of the nucleic acid-based liquid biopsies. With this aim in mind, I developed a simple and highly sensitive sandwich-type assay for detecting nucleic acids using a combination of surface-enhanced Raman scattering (SERS), which enhances Raman signals by 10^{8}– to 10^{10}–fold, and bioorthogonal Raman tags, which generate signals in the biologically silent region (1800–2800 cm^{-1}). Using gold nanorods having approximately 240 strands of oligonucleotides and 4-cyano-*N*-(2-mercaptoethyl)benzamide (4CMB) as the bioorthogonal Raman tag, target nucleic acids were successfully detected in a sequence-selective manner.

Introduction

Rapid and accurate detection of circulating biomarkers in human body fluids is key for liquid biopsies, which are non-invasive techniques for diagnosis, prognosis, determination, and prediction in clinical treatments of cancers or other diseases [1]. While the studies in search of biomarkers are under way, recent studies reveal that cell-free DNAs [2] and RNAs [3] found in body fluids, such as blood serum, saliva, and urine, have received much attention for their great potential as diagnosis biomarkers. In addition, viral DNAs [4] and RNAs [5] existing in the blood of individuals have been used to confirm the level of viremia, to make treatment decisions for viral diseases, and to monitor virus suppression by medical treatments. Besides viral DNAs and RNAs, bacterial-derived DNAs can be found in human circulation and have been used to diagnose diseases, such as systemic inflammatory and cardiovascular disease [6].

Reverse-transcription quantitative polymerase chain reaction (RT-qPCR) is the gold standard for quantifying RNAs among a number of established techniques [7,8]. RT-qPCR has been used both to quantify extremely low-abundance nucleic acids with high sequence specificity [8b] and to diagnose the various diseases [8c]. However, the processes of extracting and amplifying the target nucleic acid are cumbersome, and a highly trained staff is required to obtain consistent quantification results. For these reasons, it is not commonly used as a tool for diagnosing diseases. Therefore, highly sensitive, rapid, accurate, and simple methods for detecting nucleic acids are needed in order to establish a diagnostic method for liquid biopsies.

I focused on surface-enhanced Raman scattering (SERS), which amplifies the intensity of Raman signals of compounds adhering to metal surfaces by 10^{8}– to 10^{10}–fold, as a method for detecting biomolecules [9-11]. Raman spectroscopy has many unique features, such as providing “finger-print” information for molecular diagnosis and offering rapid and non-invasive observation of analytes. However, Raman scattering has very poor sensitivity because the process is inherently weak, with only approximately 10^{-6} photons being scattered. Over the last few decades, SERS has gained attention as a breakthrough to overcome the low sensitivity of Raman scattering. In 2002, Mirkin *et al.* reported a sandwich-type nucleic acid detection method based on SERS [12]. A DNA probe with fluorescent molecules loaded onto gold nanoparticles (gold nanoparticle probe) and a DNA probe loaded onto a glass substrate (capture probe) were prepared to sequence-selectively form a sandwich-type complex with the target DNA. After measuring the Raman signals derived from the gold nanoparticle probe, the presence or absence of the target DNA can be determined. Quantification of the signal intensity of the fluorescent molecules revealed that the detection limit of this method is 20 fM. Because of the simplicity and sensitivity of this method, sandwich-type detection is promising as a novel gold

standard method for detecting nucleic acids. Sodeoka *et al.* reported that EdU was a good Raman reporter for monitoring DNA replication in living cells because EdU had a Raman signal (at 2123 cm^{-1}) in the biologically "silent" region (1800–2800 cm^{-1}) [13]. Recently, "Click" SERS, which is a technique based on Raman scattered light splice derived from alkyne tag-conjugated gold nanoparticles, were developed by Hu *et al.* and allowed for multiplex detection of target DNAs and proteins in HeLa cells [14]. These reports indicate that bioorthogonal Raman tags that generate a signal in the biologically silent region help to avoid overlapping Raman signals of biomolecules and enable the detection of target samples with high sensitivity. In this chapter, I present a simple and facile sandwich-type method for detecting nucleic acids that combines SERS with bioorthogonal Raman tags (**Figure 1**). In this method, 4-cyano-*N*-(2-mercaptoethyl)benzamide (4CMB), which had a mercapto group for surface modification of gold nanoparticles and a cyano group as a bioorthogonal reporter group, was used as bioorthogonal Raman tags for facile and accurate identification of Raman signals. To achieve highly sensitive detection, gold nanorods (Au-NR), which are commercially available and enable a high level of SERS enhancement, were used as a SERS substrate. Partial sequences of virus DNAs, **DNA1** coding Evola virus nucleoprotein (NP) (AY058895, 1765 bp, N694–723th) and **DNA2** coding hepatitis A virus Vall7 polyprotein (AF396407, 2457 bp, N700–729th), were used as target DNAs. After capturing the target DNA on the agarose beads, Au-NR with 4CMB and thiolated DNAs were attached to the target DNA. As a result, SERS signals of 4CMB obtained from the agarose surfaces increased in response to the quantity of target DNAs.

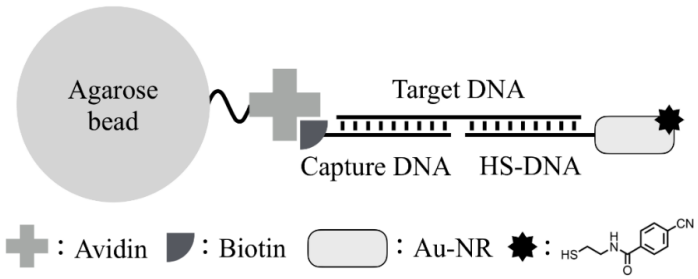

Figure 1. Schematic representation of SERS-based sandwich-type assay.

Results and discussion

The aggregation of gold nanoparticles in the presence of a salt such as NaCl is repressed by loading the oligonucleotides densely [15]. On the other hand, gold nanoparticles with high densities of the oligonucleotides showed that hybridization efficiency of DNA duplexes was very low [16,17]. It has been reported that the number of oligonucleotides introduced onto the gold nanorods was controlled by changing NaCl concentration at introducing oligonucleotides to gold nanorods [16]. To determine the suitable number of DNAs on the gold nanorods for sandwich-type assays, I evaluated the colloidal stability of the gold nanorods and hybridization efficiency of the DNAs using the gold nanorods with various numbers of DNAs on the surfaces.

First, the number of oligonucleotides on a gold nanorod was estimated according to Mirkin's procedures [16]. Gold nanorods were modified with **HS-DNA-FAM**, which was 25-mer DNA with mercapto group at 5' end and fluorescein at 3' end, at NaCl concentration of 10–500 mM to obtain the gold nanorods with various number of DNAs. Then the introduced **HS-DNA-FAM** was displaced by the addition of an excess of mercaptoethanol (final concentration: 12 mM) and was fractionated from the gold nanorods by centrifugation (7,000 rpm, 10 min) of the gold nanorods aggregates. The number of **HS-DNA-FAM** per particle was estimated from the fluorescence intensity at 520 nm of the

Table 1. Sequences of oligonucleotides used in this study.

Probe	Sequence
DNA1*	5'-GGAGTAAATGTTGGAGAACAGTATCAACAA-3'
Capture DNA1	5'-TCCAACATTTACTCCA$_{10}$-Biotin-3'
HS-DNA1	5'-HS-(CH$_2$)$_6$-A$_{10}$TTGTTGATACTGTTC-3'
DNA2*	5'-TTAGAGTTGCATGGATTAACTCCTCTTTCT-3'
Capture DNA2	5'-TCCATGCAACTCTAAA$_{10}$-Biotin-3'
HS-DNA2	5'-HS-(CH$_2$)$_6$-A$_{10}$AGAAAGAGGAGTTAA-3'
HS-DNA-FAM	5'-HS-(CH$_2$)$_6$-A$_{10}$TTGTTGATACTGTTC-FAM-3'
DNA-FAM	5'-FAM-GGAGTAAATGTTGGAGAACAGTATCAACAA-3'

***DNA1** and **DNA2** are 30-mer oligodeoxyribonucleotides coding Ebola virus nucleoprotein (NP) and hepatitis A virus Vall7 polyprotein, respectively.

supernatants and the absorbance of gold nanorods (**Figure 2**, **Table 2**). The average number of introduced **HS-DNA-FAM** increased as the concentration of NaCl increased (10 mM: 30 strands, 500 mM: 340 strands). The maximum number of DNAs on a gold nanorod with radius: 12.5 nm and length: 71 nm was predicted according to Mirkin's report [18], resulting in 290 strands of DNAs per particle, which corresponded roughly with the experimental value (340 strands per particle).

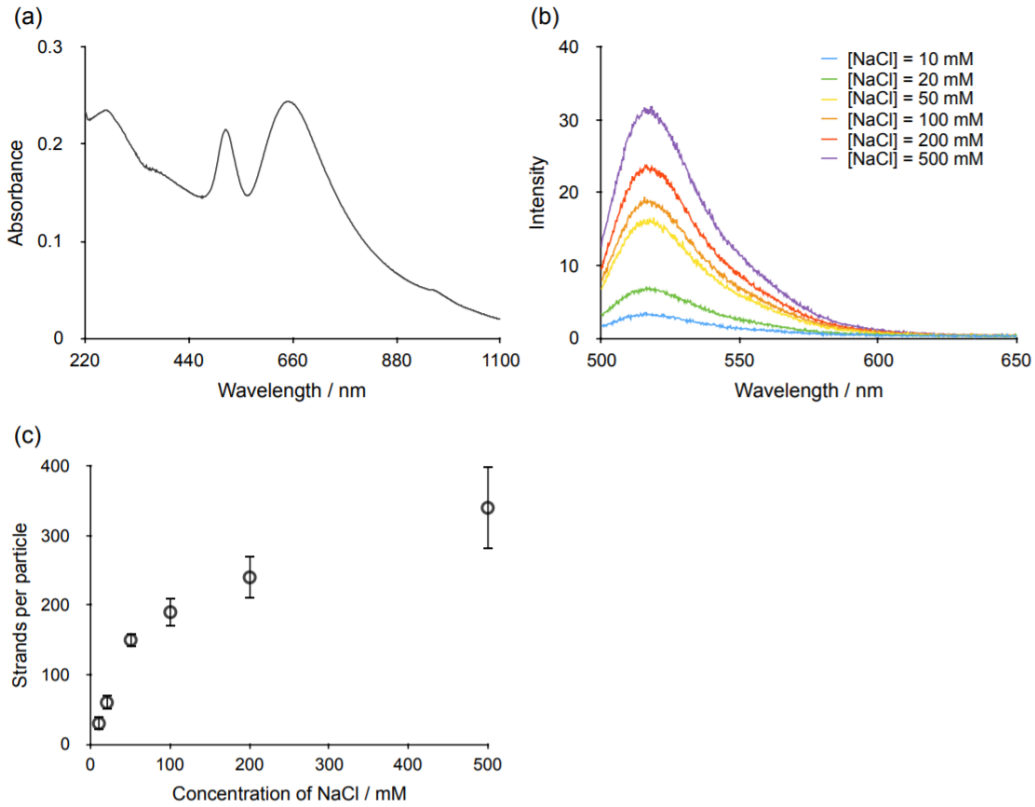

Figure 2. (a) UV spectrum of **HS-DNA-FAM** modified gold nanorods dispersed in 10 mM phosphate buffer (pH7.0) containing 0.05% SDS. (b) Fluorescence spectra of **HS-DNA-FAM** dissociated from gold nanorods by addition of mercaptoethanol. Gold nanorods with **HS-DNA-FAM** prepared by salt aging processes with various final NaCl concentrations (10-500 mM) were used for fluorescent measurements. (c) Relationship between the number of loaded-oligonucleotides on a gold nanorod and final NaCl concentration in the salt aging process. The error bars indicate the standard deviations. Buffer: 10 mM phosphate buffer (pH7.0) containing 0.05% SDS, 0.3 M NaCl and 12 mM mercaptoethanol. Band width: 3 nm (ex,em), Temperature: 20 °C.

Table 2. The number of oligonucleotides per gold nanorod.

Concentration of NaCl / mM	10	20	50	100	200	500
Strands / particle	30	60	150	190	240	340
S.D.	10	10	10	20	30	60

Next, to evaluate the colloidal stability of the DNA-modified gold nanorods at high salt concentrations, the absorptions of gold nanorods with **HS-DNA1**, which was 25-mer DNA with the 15-mer complementary sequences to **DNA1**, 10-mer spacer sequence, and mercapto group at 5' end, were measured in the following conditions: 0.1 M, 0.2 M, and 0.3 M NaCl (**Figure 3**). In the case of 0.1 and 0.2 M NaCl, all gold nanorods with **HS-DNA1** (30-340 strands / gold nanorod) were dispersed. However, in the case of 0.3 M NaCl, the gold nanorods with 30, 60, and 150 strands of **HS-DNA1** were aggregated and that with 190, 240, and 340 strands of **HS-DNA1** were dispersed.

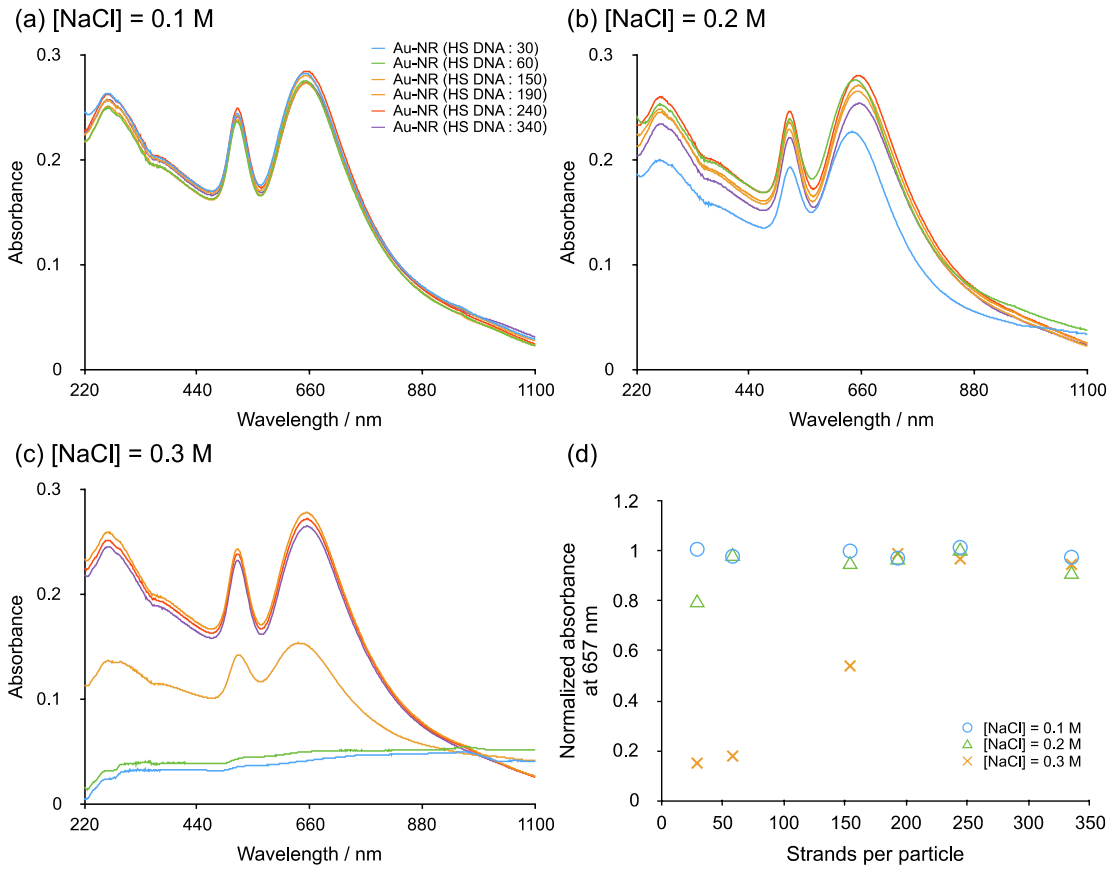

Figure 3. UV spectra of **HS-DNA1**-modified gold nanorods dispersed in 10 mM phosphate buffer (pH7.0) containing 0.05% SDS and (a) 0.1 M, (b) 0.2 M and (c) 0.3 M NaCl after incubation for 1 h at 30 °C. (d) Relationship between normalized absorbance of **HS-DNA1**-modified gold nanorods at 657 nm and the number of oligonucleotides introduced on a gold nanorod. Gold nanorods prepared by salt aging process with final NaCl concentration (blue circle: 0.1 M NaCl, green triangle: 0.2 M NaCl, orange cross: 0.3 M NaCl) were used in this study.

Then, to quantify the hybridization efficiencies of DNAs introduced onto the gold nanorod surface with target DNAs, the amount of **DNA-FAM** hybridized with **HS-DNA1** introduced onto gold nanorods was estimated. **HS-DNA1**–modified gold nanorods were mixed with 10 nM **DNA-FAM**, which was **DNA1** with fluorescein at 5' end, for 1 h in 10 mM phosphate buffer (pH7.0) containing 0.1 M, 0.2 M, and 0.3 M NaCl. Then, unhybridized **DNA-FAM** was separated from the gold nanorods by centrifugation (7,000 rpm, 10 min) and the hybridization efficiencies were estimated from the fluorescent intensity of supernatants at 520 nm (**Figure 4**). The hybridization efficiencies of the DNAs immobilized onto the gold nanorods were improved by increasing NaCl concentration in the same manner as the DNA hybridization in solution phase. Gold nanorods with 340-strands of **HS-DNA1** showed lower efficiency than that with 190- and 240-strands of **HS-DNA1** due to the condensed charge of the gold nanorod surfaces by hybridization. In particular, at the concentration of 0.3 M NaCl, **DNA-FAM** was most efficiently captured by gold nanorods with 240 strands of **HS-DNA1**

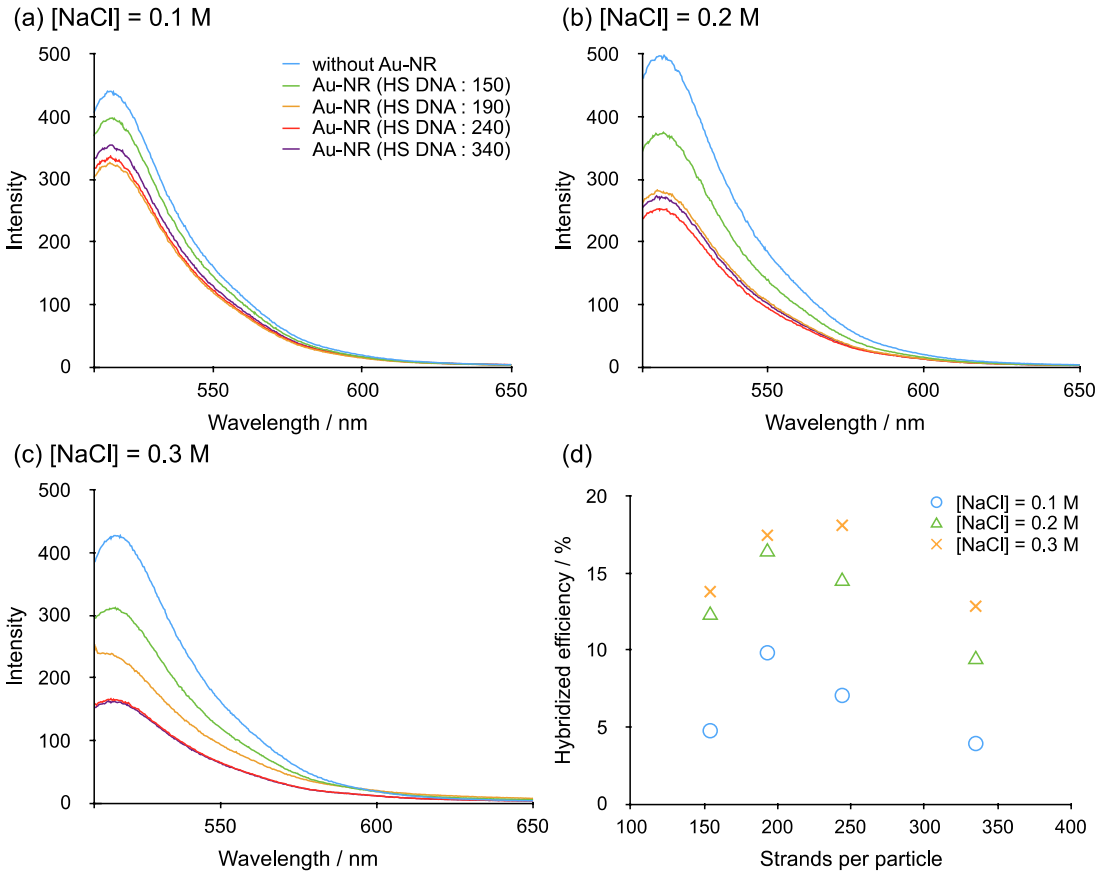

Figure 4. Fluorescence spectra of supernatant after incubation of **HS-DNA1**-modified gold nanorods and **DNA-FAM** for 1 h at 30 °C in 10 mM phosphate buffer (pH7.0) containing 0.05% SDS and (a) 0.1 M, (b) 0.2 M and (c) 0.3 M NaCl. (d) Hybridized efficiency of **HS-DNA1** introduced on the gold nanorods with **DNA-FAM** as a function of the number of **HS-DNA1** introduced on the gold nanorods. The Hybridized efficiencies were obtained as follows: (the number of **DNA-FAM** hybridized with **HS-DNA1**) / (the number of **HS-DNA1** introduced on the gold surface). Blue circle: 0.1 M NaCl, Green triangle: 0.2 M NaCl, Orange cross: 0.3 M NaCl.

(hybridized efficiency at 190 strands: 17%, 240 strands: 18%, 340 strands: 13%). On the basis of these experimental results, gold nanorods with 240 strands of **HS-DNA1** were estimated to be useful for sandwich-type assays for detecting target nucleic acids.

Bioorthogonal SERS probes composed of a gold nanorods, 4CMB, and HS-DNAs were prepared using the procedure shown in **Scheme 1**. 4-cyano-*N*-(2-mercaptoethyl)benzamide (4CMB) was synthesized from 4-cyanobenzoic acid as shown in **Scheme 2**. *N*,*N'*-bis(4-cyanobenzoyl)cystamine, oxidized 4CMB, was synthesized by condensation of cystamine and 4-cyanobenzoic acid. 4CMB was prepared by reduction of *N*,*N'*-bis(4-cyanobenzoyl)cystamine with tris(2-carboxyethyl)phosphine (TCEP). Without purification, the reaction mixture containing 4CMB and TCEP was directly added to the dispersions of **HS-DNA1**– or **HS-DNA2**–modified gold nanorods in 10 mM phosphate buffer (pH7.0) and incubated at 30 °C for 1 day. The introduction of 4CMB onto the gold nanorod surfaces was verified by Raman measurements (**Figure 5b**). The Raman spectrum of prepared SERS probes excited at 785 nm had Raman bands corresponding to 4CMB (1188 cm^{-1} (δCH), 1289 cm^{-1} (νPh), 1616 cm^{-1} (νPh), 1646 cm^{-1} (νC=O), 2237 cm^{-1} (νC≡N)). As the spectrum indicates, a single Raman band of the nitrile group was observed in the silent region. Although, the Raman band of the nitrile group in SERS probes was broader than that in *N*,*N*'-bis(4-cyanobenzoyl)cystamine, the Raman shift of the nitrile group had the same wavenumber in both the SERS probes and *N*,*N*'-bis(4-cyanobenzoyl)cystamine (**Figure 5**). These results suggest that 4CMBs are immobilized onto the gold nanorod surfaces.

For sandwich-type assay, agarose beads functionalized with anchor DNAs were also prepared as follows: **Capture DNA1** and **Capture DNA2** having 25-mer DNA with 15-mer complementary sequence of **DNA1** and **DNA2**, respectively, 10-mer spacer sequence, and biotin at 3' end were used as anchor DNAs. These Capture DNAs were mixed with avidin-coated agarose beads for 1 h to immobilize onto agarose beads through avidin-biotin binding. The amounts of Capture DNAs immobilized on the agarose beads were estimated from the absorption spectra of reaction mixture (ca. 26 fmol / particle, **Figure 6**).

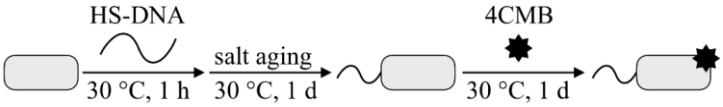

Scheme 1. Preparation of SERS probes.

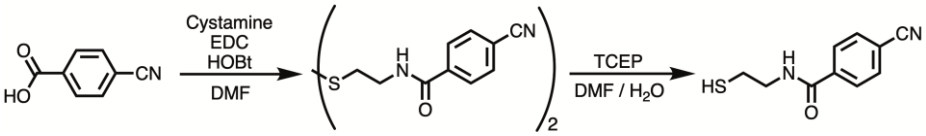

Scheme 2. Synthetic scheme of 4-cyano-*N*-(2-mercaptoethyl)benzamide.

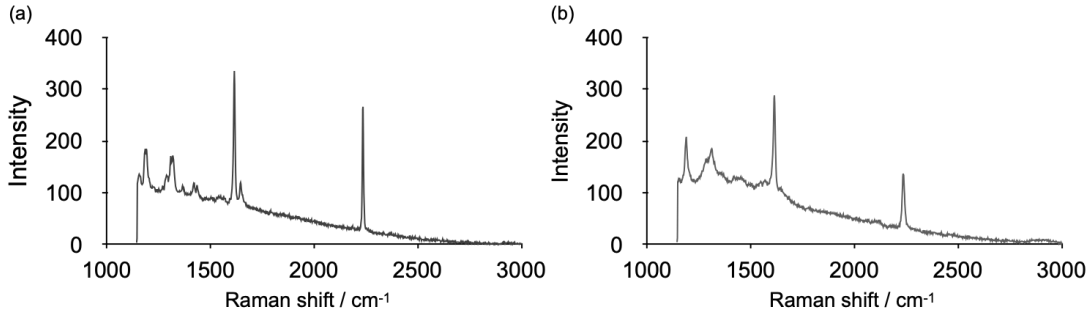

Figure 5. Raman spectra of (a) *N*,*N*'-bis(4-cyanobenzamido)cystamine and (b) the SERS probe at 785 nm of excitation wavelength. Laser: 785 nm, Grating: 300 cm^{-1}, Exposure time: 5 s, Objective lens: x50, ND filter (Power): (a) 20% (19.6 mW), (b) 100% (86.4 mW).

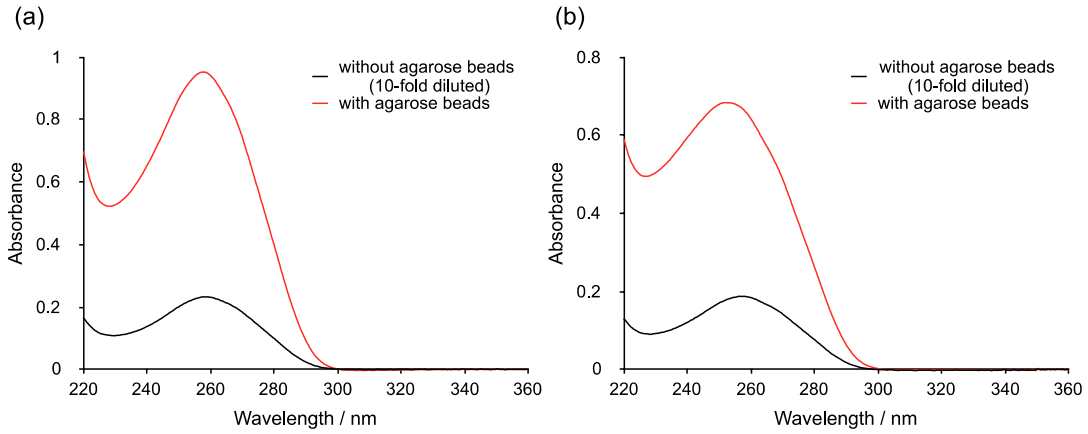

Figure 6. UV spectra of supernatant after centrifugation of mixture of Capture DNAs ((a) **Capture DNA1,** (b) **Capture DNA2)** stirred for 10 min at rt in 10 mM phosphate buffer (pH7.0) containing 0.1 M NaCl in the (red) presence or (black) absence of avidin-modified agarose beads.

I prove the concept of sandwich-type assays for detecting target nucleic acids using SERS probes and agarose beads with anchor DNAs as shown in **Figure 1**. Target DNA and probe sequences were the same as previously reported sequences by Mirkin *et al*. [12] and the melting temperatures of the DNA duplexes, **DNA1**/**HS-DNA1**, **DNA2**/**HS-DNA2**, **DNA1**/**Capture DNA1**, and **DNA2**/**Capture DNA2**, in 10 mM phosphate buffer (pH7.0) containing 0.3 M NaCl and 0.05% SDS were 55.3 ± 0.5, 52.3 ± 0.4, 55.3 ± 0.1, and 47.0 ± 0.4, respectively. After mixing the SERS probes and the agarose beads with an excess amount of anchor DNAs for 1 h in the presence or absence of 1 nM target DNAs in 10 mM phosphate buffer (pH7.0) containing 0.3 M NaCl and 0.05% SDS, the Raman spectra of the fractionated agarose beads were measured and a peak area of Raman signal derived from the nitrile group was used for quantification of the DNAs (**Figure 7**). In the case of the probe set for **DNA1**, the strong Raman signal of the nitrile group was clearly observed in the presence of **DNA1**, whereas a faint peak was observed in the presence of **DNA2** and in the absence of DNAs. The Raman peak areas significantly increased in the presence of target DNAs compared to that in the absence of target DNAs (**DNA1**: 10-fold, **DNA2**: 7-fold). Additionally, noncomplementary DNAs hardly increased the corresponding Raman peak area. These results indicate that target DNAs can be discriminated from DNAs with random sequences by the sandwich-type assay using the bioorthogonal SERS probes.

Finally, the limit of detection (LOD) of the sandwich-type assay were evaluated. **DNA1** or **DNA2** ranging from 0 M to 2 nM was added to the solution of the agarose beads with anchor DNAs and SERS probes for **DNA1** and **DNA2**, respectively, and incubated for 1 h in 10 mM phosphate buffer (pH7.0) containing 0.3 M NaCl and 0.05% SDS. In the case of **DNA1**, an increase in Raman peak area of the nitrile group was observed at the concentration of 500 pM, while in the case of **DNA2**, the increase occurred at 1 nM (**Figure 8**). Therefore, the LOD of the sandwich-type assay for **DNA1** and **DNA2** were determined to be 500 pM and 1 nM, respectively.

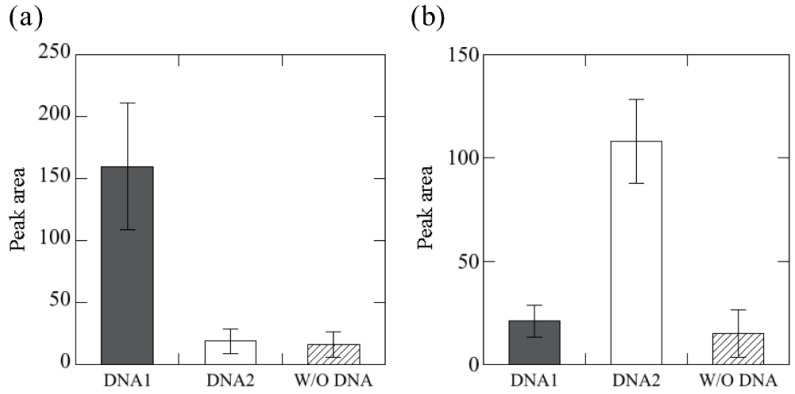

Figure 7. Peak area derived from the Raman tag on the bead surface used in the sandwich-type assay for (a) **DNA1** and (b) **DNA2** in the presence of **DNA1** (gray bar) and **DNA2** (open bar) and in the absence of target DNA (hatched bar). The error bars indicate the standard deviations calculated from five measurements.

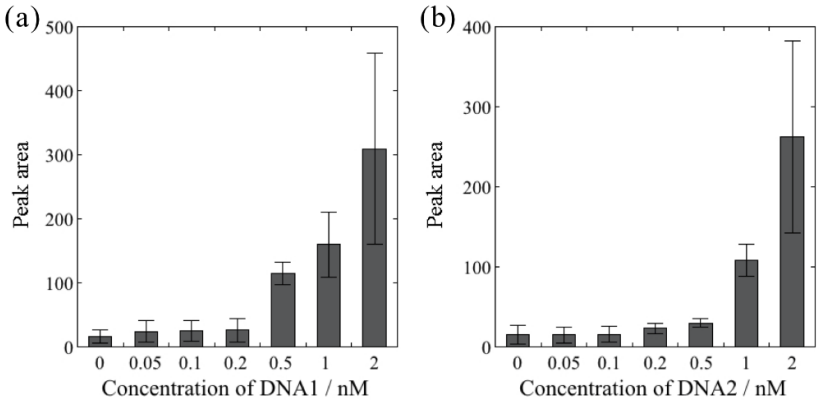

Figure 8. The assay results obtained for seven different concentrations of target DNAs using the sandwich-type assay for (a) **DNA1** and (b) **DNA2**. The error bars indicate the standard deviations calculated from five measurements.

Conclusion

I prepared bioorthogonal SERS probes composed of gold nanorods with bioorthogonal Raman tags having a Raman signal in the biologically silent region (1800–2800 cm^{-1}) and HS-DNAs (approximately 240 strands), and demonstrated the sequence-selective and sensitive detection of target DNAs using the SERS probes in the sandwich-type assay. By this assay, target DNAs were successfully detected in a sequence-selective manner with a detection limit of 500 pM.

Materials and methods

Materials and instrumentation. Reagents, solvents, and oligonucleotides were purchased from commercial sources. NMR spectra were recorded on a 300 MHz NMR spectrometer (Bruker: AVANCE II 300). The ESI-TOF-MS (Bruker: micro TOF LC) was used to monitor the reduction reaction of a disulfide bond. A UV-Vis spectrometer (Shimadzu: UV-1800) was used to evaluate the concentrations of DNAs and gold nanorods. A fluorescence spectrometer (Shimadzu: RF-5300PC) was used to estimate the concentrations of fluorescein-modified DNAs. All Raman measurements were carried out by a micro-Raman spectroscope (Nanophoton: RAMAN-11).

Synthesis of 4-cyano-*N*-(2-mercaptoethyl)benzamide. *N*,*N'*-bis(4-cyanobenzoyl)cystamine (5.6 nmol) and tris(2-carboxyethyl)phosphine hydrochloride (570 nmol) were dissolved in *N*,*N*-dimethylformamide (90 μL) and sterile water (10 μL) and stirred at 30 ºC for 3 h. The product of the reduction reaction was monitored by ESI-TOF-MS spectrometry. The reaction mixture was used for next reactions without purifications. HRMS (ESI-TOF-MS) *m/z*: $[M–H]^-$ calcd for $C_{10}H_9N_2OS$ 205.04, found 205.09.

Introduction of thiolated oligonucleotides on the gold nanorods. Because mercapto groups introduced to oligonucleotides tends to form disulfide bond after long storing, thiol-modified oligonucleotides were first treated with reductive reagents before use. Thiol-modified oligonucleotides (5.7 nmol) and tris(2-carboxyethyl)phosphine hydrochloride (570 nmol) were dissolved in sterile water (100 μL). The reaction mixture was incubated at 30 ºC for 3 h. The reaction mixture was then purified by a NAP-5 column. The product of the reduction reaction was analyzed by ESI-TOF-MS spectrometry. HRMS (ESI-TOF-MS) *m/z*: $[M–5H]^{5-}$ calcd for **HS-DNA-FAM** 1690.49, found 1690.58; $[M–5H]^{5-}$ calcd for **HS-DNA1** 1576.67, found 1576.64. $[M–5H]^{5-}$ calcd for **HS-DNA2** 1603.49, found 1603.45. The purified oligonucleotides (250 pmol) we
re added to gold nanorods (25 fmol) in 250 μL of 10 mM phosphate buffer (pH7.0) containing 0.05% SDS at 30 ºC for 1 h. Then, concentrations of NaCl were increased to 10 mM, 20 mM, 50 mM, 100 mM, 200 mM, and 500 mM by salt aging processes to compensate the negative charge of oligonucleotides. To prepare 10 mM and 20 mM of NaCl, 1 M NaCl was added dropwise to the reaction mixtures until the desired NaCl concentration. For 50 mM of NaCl, 4 M NaCl was added dropwise to the reaction mixture until desired NaCl concentration. For 100–500 mM of NaCl, 4 M NaCl was gradually added (up to 100 mM of NaCl: 50 mM increments / 30 min, from 200 mM to 500 mM of NaCl: 100 mM increments / 30 min) until desired NaCl concentration. After the salt aging

process, the reaction mixture was incubated at 30 ºC overnight, then centrifuged at 7,000 rpm for 10 min and the supernatant was removed to a final volume of 50 μL. The pellet was redispersed in 10 mM phosphate buffer (pH7.0) containing 0.05% SDS to a final volume of 250 μL. The gold nanorods were subjected to four cycles of centrifugation and redispersion. Lastly, the gold nanorod dispersion was enriched to a final volume of 50 μL by removal of the supernatant after centrifugation.

Quantification of the number of oligonucleotides on a gold nanorod. HS-DNA-FAM–modified gold nanorods (20 fmol) were added to mercaptohexanol (3.6 μmol) in 300 μL of 10 mM phosphate buffer (pH7.0) containing 0.05% SDS and 0.3 M NaCl at 30 ºC for 1 h. After incubation, the reaction mixtures were centrifuged at 7,000 rpm for 10 min and the supernatants were collected. Concentration of dissociated **HS-DNA-FAM** in the supernatants was calculated using the fluorescence intensity at 520 nm. From these values, the number of **HS-DNA-FAM** on a gold nanorod was estimated.

Preparation of SERS probes. Gold nanorods (25 fmol) with approximately 240 strands of **HS-DNA1** or **HS-DNA2** were added to 4CMB (250 pmol) in 250 μL of 10 mM phosphate buffer (pH7.0) containing 0.05% SDS at 30 ºC for 1 day. The reaction mixture was centrifuged at 7,000 rpm for 10 min and the supernatant was removed to a final volume of 50 μL. The pellet was redispersed in 10 mM phosphate buffer (pH7.0) containing 0.05% SDS to a final volume of 250 μL. The gold nanorods were subjected to four cycles of centrifugation and redispersion. The gold nanorod dispersion was enriched to a final volume of 50 μL by centrifugation and removal of the supernatant.

Preparation of agarose beads with capture DNA. Avidin-modified agarose beads (40,000 particles) were mixed with **Capture DNA1** or **Capture DNA2** (2 nmol) in 250 μL of 10 mM phosphate buffer (pH7.0) containing 0.1 M NaCl for 10 min at rt. The reaction mixture was centrifuged at 7,000 rpm for 1 min, and 200 μL of the supernatant was collected and measured by UV-Vis spectroscopy. The numbers of **Capture DNA1** or **Capture DNA2** introduced on an agarose bead were estimated from the decrease in absorbance at 260 nm. The pellet of agarose beads was redispersed in 200 μL of 10 mM phosphate buffer (pH7.0) containing 5% skim milk, 0.05% Tween 20, and 0.1 M NaCl followed by vigorous stirring for 1 h at rt. The reaction mixture was centrifuged at 7,000 rpm for 1 min and the supernatant was removed to a final volume of 50 μL. The pellet was redispersed in 10 mM phosphate buffer (pH7.0) to a final volume of 250 μL. The agarose beads were subjected to five cycles of centrifugation and redispersion, and agarose beads with DNA capacity (ca. 26 fmol / particle) were obtained.

Sandwich-type assay. The target DNAs were added to the agarose beads (2,700 particles) with **Capture DNA1** or **Capture DNA2** and SERS probes (200 fmol) for **DNA1** or **DNA2** in 100 μL of 10

mM phosphate buffer (pH7.0) containing 0.05% SDS and 0.3 M NaCl at rt for 1 h. After mixing, the reaction mixture was filtrated to separate the agarose beads from surplus SERS probes. The fractionated agarose beads were washed three times with 100 μL of 10 mM phosphate buffer (pH7.0) containing 0.3 M NaCl and 0.05% SDS and recovered with 50 μL of 10 mM phosphate buffer (pH7.0). Raman spectra of the dried agarose beads were measured by micro-Raman spectroscopy.

References

[1]. (a) Crowley, E.; Nicolantonio, F. D.; Loupakis, F.; Bardelli, A. *Nat. Rev. Clin. Oncol.* **2013**, *10*, 472–484. (b) Krebs, M. G.; Metcalf, R. L.; Carter, L.; Braby, G.; Blackhall, F. H.; Dive C. *Nat. Rev. Clin. Oncol.* **2014**, *11*, 129–144. (c) Matsuzaki, J.; Ochiya, T. *J. Clin. Biochem. Nutr.* **2018**, *63*, 6–11.

[2]. Daniūnaitė, K.; Jarmalaitė, S.; Kriukienė, E. *Curr. Opin. Biotechnol.* **2018**, *55*, 23–29.

[3]. (a) Endzeliņš, V.; Melne, V.; Kalņa, Z.; Lietuvietis, V.; Riekstiņa, U.; Llorente, A.; Linē, A. *Mol. Cancer* **2016**, *15*, 41. (b) Ono, S.; Lam, S.; Nagahara, M.; Hoon, D. S. *J. Clin. Med.* **2015**, *4*, 1890–1907.

[4]. Wang, L.; Xu, X.; Zhang, H.; Qian, J.; Zhu, J. *Virol. J.* **2015**, *12*.

[5]. (a) Moritou, Y.; Ikeda, F.; Takeuchi, Y.; Seki, H.; Nanba, S.; Iwasaki, Y.; Yamamoto, K. *J. Clin. Microbiol.* **2014**, *52*, 544–548. (b) Lu, F.; Wang, J.; Chen, X.; Xu, D.; Xia, N. *Front. Med.* **2017**, *11*, 502–508.

[6]. Szeto, C. C.; Kwan, B. C.; Chow K. M.; Kwok, J. S.; Lai, K. B.; Cheng, P. M.; Pang, W. F.; Ng, J. K.; Chan, M. H.; Lit, L. C.; Leung, C. B.; Li, P. K. *PLoS One* **2015**, *10*, e0125162.

[7]. (a) Graybill, R. M.; Bailey, R. C. *Anal. Chem.* **2016**, *88*, 431–450. (b) Dong, H.; Lei, J.; Ding, L.; Wen, Y.; Ju, H.; Zhang, X. *Chem. Rev.* **2013**, *113*, 6207–6233.

[8]. (a) Raymond, C. K.; Roberts, B. S.; Garrett-Engele, P.: Lim, L. P.; Johnson, J. M. *RNA* **2005**, *11*, 1737–1744. (b) Johnson, B. N.; Mutharasan, R. *Analyst* **2014**, *139*, 1576–1588. (c) Olney, R. C.; Mougey, E. B. *Mol. Cell. Endocricol.* **1999**, *156*, 63–71.

[9]. (a) Fleischmann, M.; Hendra, P. J.; McQuilla, A. *J. Chem. Phys. Lett.* **1974**, *26*, 163–166. (b) Campion, A.; Kambhampati, P. *Chem. Soc. Rev.* **1998**, *27*, 241–250.

[10]. Wang, Y.; Yan, B.; Chen, L. *Chem. Rev.* **2013**, *113*, 1391–1428.

[11]. Camden, J. P.; Dieringer, J. A.; Zhao, J.; Van Duyne, R. P. *Acc. Chem. Res.* **2008**, *41*, 1653–1661.

[12]. Cao, Y. C.; Jin, R.; Mirkin, C. A. *Science*, **2002**, *297*, 1536–1540.

[13]. Yamakoshi, H.; Dodo, K.; Okada, M.; Ando, J.; Palonpon, A.; Fujita, K.; Kawata, S.; Sodeoka, M. *J. Am. Chem. Soc.* **2011**, *133*, 6102–6105.

[14]. Zeng, Y.; Ren, J. Q.; Shen, A. G.; Hu, J. M. *J. Am. Chem. Soc.* **2018**, *140*, 10649–10652.

[15]. Liu, B.; Liu, J. *Anal. Methods* **2017**, *9*, 2633–2643.

[16]. Demers, L. M.; Mirkin, C. A.; Mucic, R. C.; Reynolds, R. A. III; Letsinger, R. L.; Elghanian, R.; Viswanadham, G. *Anal. Chem.* **2000**, *72*, 5535–5541.

[17]. Akamatsu, K.; Kimura, Mio.; Shibata, Y.; Nakano, S.; Miyoshi, D.; Nawafune, H.; Sugimoto, N. *Nano Lett.* **2006**, *6*, 491–495.

[18]. Hill, H. D.; Millstone, J. E.; Banholzer, M. J.; Mirkin. C. A. *ACS Nano* **2009**, *3*, 418–424.

Chapter 2

Ratiometric SERS assays for reliable and automatic quantification of nucleic acids

Abstract: I developed a novel ratiometric assay for the facile and accurate quantification of nucleic acids using two kinds of bioorthogonal Raman reporters attached to SERS (surface-enhanced Raman scattering) probes. Normalization of the SERS signal intensities of a phenylethynylphenyl (PEP) group by ethynylphenyl (EP) group allows the automatic and facile quantification of target nucleic acids down to 86 pM.

Introduction

Nucleic acid detection methods play key roles in the diagnosis of serious diseases, such as viral diseases, inherited diseases, and cancers [1,2]. Quantitative polymerase chain reaction is the gold standard among conventional methods for quantifying nucleic acids with high sensitivity [3]. However, quantitative polymerase chain reaction has been poorly utilized for the diagnosis of several diseases since the enzymatic amplification of nucleic acids is complicated and time-consuming procedure. Thus, novel diagnostic techniques that do not require the enzymatic amplification of target nucleic acids are required.

SERS (surface-enhanced Raman scattering), in which localized surface plasmon resonance amplifies weak Raman signals by 10^8- to 10^{11}-fold, has attracted much attention as a highly sensitive vibrational spectroscopy technique [4,5]. SERS has attracted considerable interest in biomedical fields, such as cell imaging and biomolecular sensing [6]. Until now, SERS-based assays have been developed for detecting biomolecules of interest, such as small molecules [7,8], proteins [9,10], and nucleic acids [11-13]. However, SERS-based assays present major challenges for the reliable and accurate quantification of target molecules using automatically collected Raman spectra due to the poor reproducibility of SERS signals. This problem seems to derive from two factors: (1) the random aggregation of metal nanoparticles such as gold nanoparticles yields high standard deviations of the SERS intensities [14-16]; (2) the localized surface plasmon enhancement of electromagnetic fields depends on the measurement conditions, for example, fluctuation of laser power and loss of focus [6,17-19]. For these reasons, highly technical experts are required for the accurate SERS measurement in the conventional SERS-based assays. Therefore, SERS-based sensing strategies that enable us to simply and easily detect target molecules are required for the development of general-purpose or automatic detection methods.

Recently, to address these problems, SERS-based ratiometric assays using internal standard have been developed [20-22]. In 2017, Yu and coworkers reported a ratiometric SERS aptasensor composed of a gold nanoparticle with 3'-Rox-labeled complementary DNA and 3'-Cy5-labeled ATP-binding aptamer for quantifying ATP [15]. In 2019, Wu and coworkers presented SERS-based assays for quantifying microRNA using a combination of catalytic hairpin assembly and a SERS biosensor composed of Ag-NPs–coated silica plates, capture DNA, and 4-ATP as an internal standard [23]. These reports indicate that the introduction of an internal standard into SERS-based assays allows to improve the reproducibility of SERS signals and accurately quantify target molecules. In 2011, Sodeoka and coworkers reported the first Raman imaging of nuclear localization in living cells using EdU, which had a Raman signal in the biologically silent region (1800–2800 cm^{-1}) [24]. Recently, Li and

coworkers reported gold nanorods modified with PEB (3-(4-(phenylethynyl)benzylthio)propanoic acid)–tagged peptides and TPA (4-thiol phenylacetylene), from which two kinds of Raman signals were derived (at 2218 cm^{-1} and 2027 cm^{-1}, respectively), for ratiometric SERS imaging of caspase 3 in live cells and tissues [25]. These reports suggest that bioorthogonal Raman reporters allows for the sensitive and easy detection of target molecules in biological samples. However, to our knowledge, there has been little study of ratiometric SERS assays that can easily and accurately quantify nucleic acids using bioorthogonal Raman reporters in automatically selected Raman spectra.

Previously, I developed a facile and simple sandwich-type assay for the detection of nucleic acids using bioorthogonal SERS probes composed of gold nanorods with 5'-thiolated DNA and 4CMB (4-cyano-*N*-(2-mercaptoethyl)benzamide) as the bioorthogonal Raman reporter [26]. SERS probes and Capture DNAs introduced on the agarose beads were prepared to form a sandwich complex with the target DNAs in a sequence-selective manner. In this assay, 500 pM target DNAs were successfully detected (see chapter 1).

In this chapter, I developed an automated ratiometric SERS assay for the facile and reliable quantification of nucleic acids using bioorthogonal SERS probes composed of Au-NSs (gold nanostars), whose LSPR (localized surface plasmon resonance) wavelengths are easy to tune and enable a high level of SERS enhancement, and two types of bioorthogonal Raman reporters. In this study, partial sequences of DNA, **cDNA**, coding Ebola virus NP (nucleoprotein) (AY058895, 1765 bp, N694–723th) were used as targeted DNAs. Thiolated DNAs, **5'-HS-DNA** and **3'-HS-DNA**, were a 25-mer DNA with the 15-mer complementary sequences to **cDNA**, the 10-mer spacer sequences, and a mercapto group at the 5'-end and 3'-end, respectively [26,27]. EP (*N*-(4-ethynylphenyl)-3-mercaptopropanamide) and PEP (3-mercapto-*N*-[4-(2-phenylethynyl)phenyl]propenamide) as bioorthogonal Raman reporters, each of which generates a Raman signal in the biologically silent region, were used for facile identification of Raman signals derived from Raman reporters. A schematic diagram of ratiometric SERS assays using SERS probes is shown in **Figure 1**. I prepared two types of bioorthogonal SERS probes, each of which consisted of Au-NSs, thiolated DNAs, and bioorthogonal Raman reporters (**Figure 1a**). **SERS probe 1** was prepared by modifying **5'-HS-DNA**, PEP, and MCH (mercaptohexanol) as a backfill to Au-NSs. **SERS probe 2** was prepared by modifying **3'-HS-DNA** and EP to Au-NSs, and adsorbed onto amino-modified silica beads (**SERS probe 2**-coated silica bead). Procedures for the detection of **cDNA** using **SERS probe 1** and **SERS probe 2**-coated silica bead were separated into two steps (**Figure 1b**): (1) **SERS probe 1** was captured onto **SERS probe 2**-coated silica bead through a sandwich-type complex with the **cDNA**, and the complexes on the silica beads were separated from the surplus of **SERS probe1** by filtration. (2) After sonication of the isolated silica beads for 20 sec, the complexes were liberated and isolated from the silica beads. The solution of sandwich-type complexes was dried on a glass slide, and the SERS signals of **SERS probe 1** and **SERS probe 2** were concomitantly obtained by Raman measurements.

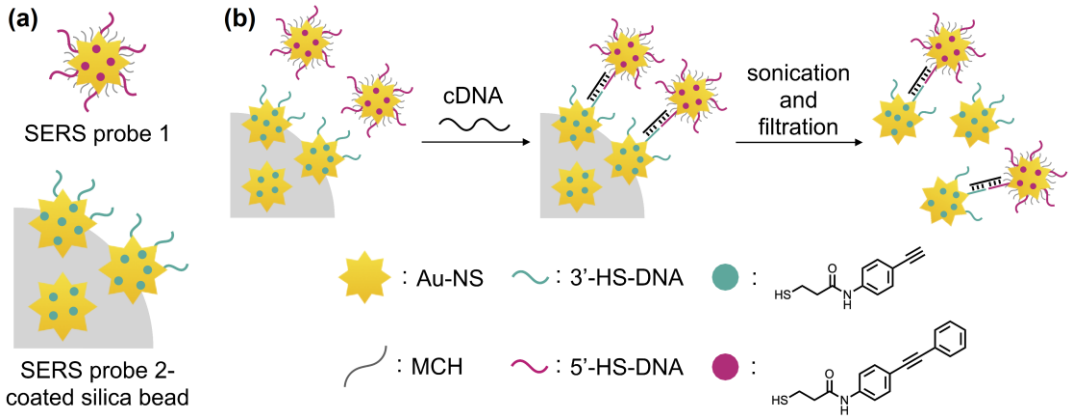

Figure 1. Schematic diagram of ratiometric SERS assay for quantifying nucleic acids. (a) **SERS probe 1** and **SERS probe 2**-coated silica bead for ratiometric SERS assays. (b) Procedures for quantifying **cDNA** by ratiometric SERS assay.

Table 1. Sequence of oligonucleotides used in this study.

Probe	Sequence
cDNA*	5'-GGAGTAAATGTTGGAGAACAGTATCAA CAA-3'
3'-HS-DNA	5'-TCCAACATTTACTCCA$_{10}$-(CH$_2$)$_3$-SH-3'
5'-HS-DNA	5'-HS-(CH$_2$)$_6$-A$_{10}$TTGTTGATACTGTTC-3'
rDNA*	5'-TTAGAGTTGCATGGATTAACTCCTCTT TCT-3'
HS-DNA-F	5'-FAM-GGAGTAAATGTTGGAGAACAG TATCAACAA-3'

*__cDNA__ and __rDNA__ consisting of partial sequence of DNA coding Ebola virus NP and hepatitis A virus polyprotein, respectively.

Results and discussion

A SERS enhancement is dependent on the LSPR wavelength of metal nanostructures, such as nanoparticles, nanorods, nanoprisms, and nanostars [28,29]. Recently, Au-NSs have been used for SERS-based detection methods [30-33] because the LSPR wavelength of Au-NSs is readily tuned [34-36] and Au-NSs enable us to strongly enhance Raman signals [29]. Therefore, in this study, Au-NSs are used as SERS substrates. Au-NSs were prepared by seed-mediated synthesis methods [37,38]. In these methods, metal seeds (gold or silver seeds) were used as nucleation points where auric ion adsorbs for branch growth. In particular, Au-NSs are synthesized in high yields in the case of silver seeds [37]. Accordingly, the silver seeds were used for synthesis of Au-NSs with the suitable LSPR wavelength for excitation by laser (Laser wavelength: 785 nm). First, silver seeds were synthesized by reduction of silver nitrate using sodium borohydride and trisodium citrate. Second, Au-NSs were prepared by growth of the prepared silver seeds with tetrachloroauric acid, silver nitrate, and L-ascorbic acid, and then stabilized with PSS (polystyrene sulfonic acid) as a surfactant. PSS-coated Au-NSs were converted into citrate-coated Au-NSs by a surfactant-exchange method with citrate [39]. The shapes and sizes of the silver seeds and citrate-coated Au-NSs were observed in TEM (transmission electron microscopy) (**Figure 2a,b**). TEM images showed that the diameters of the silver seeds and Au-NSs were 13.5 ± 2.1 nm and 111.5 ± 11.7 nm, respectively, and that Au-NSs had a star shape. The optical properties were analyzed by UV-Vis (ultraviolet visible absorption spectroscopy) (**Figure 2c**). The silver seeds showed a narrow range of LSPR wavelengths (388 nm) with a yellow color, whereas the PSS-coated Au-NSs and citrate-coated Au-NSs showed a wide range of LSPR wavelengths (700–900 nm) with a greenish-blue color. The LSPR absorbance maximum of citrate-coated Au-NSs was blue-shifted from 788 nm to 775 nm by the exchange of PSS to citrate. Because the LSPR wavelengths of prepared Au-NSs were located between 750 and 800 nm, they were suitable to excite with laser at 785 nm. To identify the molecules adsorbed onto the Au-NSs, Raman spectra of PSS- and citrate-coated Au-NS pellets were measured (**Figure 2d**). Displacements of PSS by adding citrate lead to a decrease in the signal intensity of νSO_3^- (1133 cm^{-1}) and increases in those of νCCO *trans* (967 cm^{-1}), νCO_2^- *sym* + δCH_2 + ωCH_2 (1378 cm^{-1}), and νCO_2^- *asym* (1586 cm^{-1}). These results indicate that PSS adsorbed onto Au-NSs is converted to citate by this surfactant-exchange method.

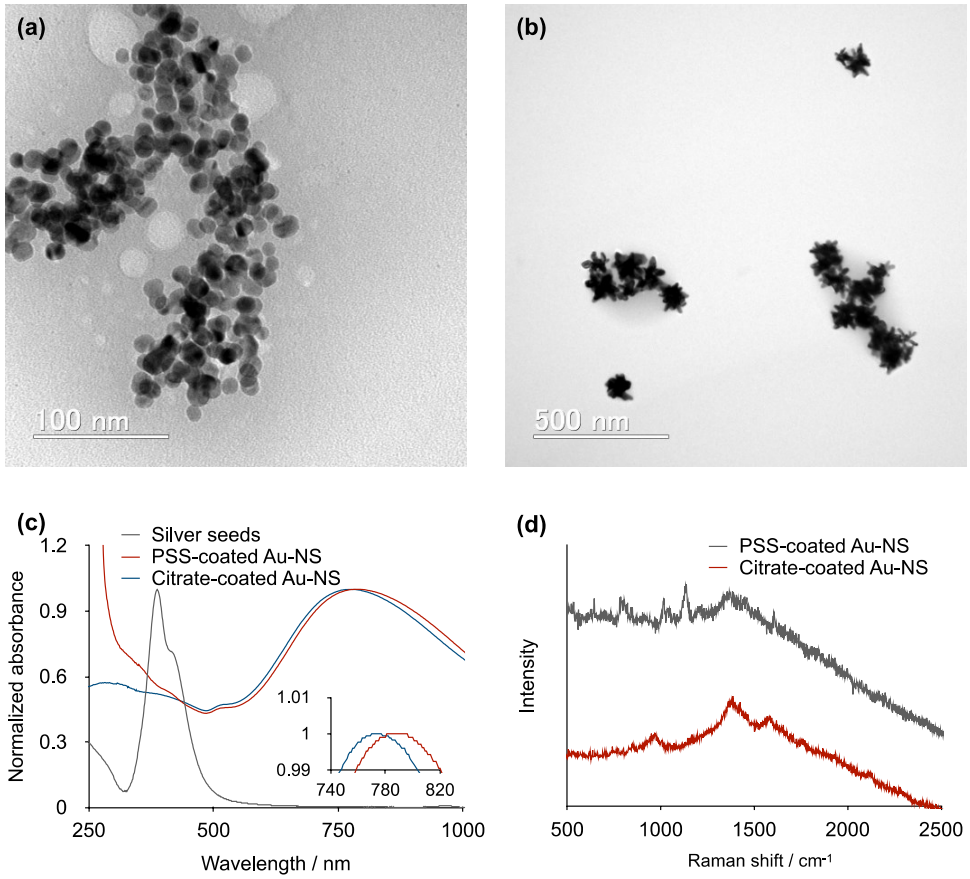

Figure 2. TEM images of (a) silver seeds and (b) citrate-coated Au-NSs. Scale bar: (a) 100 nm, (b) 500 nm. (c) UV-Vis spectra of (gray) silver seeds, (red) PSS-coated Au-NSs and (blue) citrate-coated Au-NSs. The inset shows a zoom for a wavelength between 740 and 820 nm. (d) Raman spectra of (gray) PSS-coated Au-NSs and (red) citrate-coated Au-NSs with 785 nm of excitation wavelength.

Next, the bioorthogonal Raman reporters (EP and PEP) were synthesized as shown in **Scheme 1,2**. Thiol groups were used for modifying metallic nanostructure surfaces because of the strong adsorption onto a metallic surface. 3MPA (3-mercaptopropionic acid), which was adsorbed on the gold surface and functionalized with aniline derivatives, was used as a Raman reporter backbone. In this study, Raman reports were synthesized starting from DTDPA (3,3'-dithiodipropionic acid), oxidized 3MPA. EP dimer (3,3'-Dithiobis[*N*-(4-ethynylphenyl)propanamide]) and PEP dimer (3,3'-dithiobis{*N*-[4-(2-phenylethynyl)phenyl]propanamide}) as a bioorthogonal Raman reporter dimer were prepared by condensation between DTDPA and aniline derivatives (i.e., 4-ethynylaniline and 4-(2-phenylethynyl)aniline). These Raman reporter dimers in the solid state were characterized by Raman measurements (laser wavelength: 785 nm) (**Figure 3**). EP dimer and PEP dimer emitted a major Raman signal in the silent region corresponding to the ethynyl group (EP dimer: 2112.22 cm^{-1} (νC≡C), PEP dimer: 2231.29 cm^{-1} (νC≡C)). Raman reporters were prepared by reduction of Raman reporter dimers with TCEP (tris(2-carboxyethyl)phosphine) and the reduction reaction was identified by ESI-TOF-MS. After reducing Raman reporter dimers for 3 h, the peaks of Raman reporters were observed, whereas those of Raman reporter dimers completely disappeared (ESI-TOF-MS *m/z*: $[M–H]^-$ calcd for EP 204.0483, found 204.0495, $[M–H]^-$ calcd for PEP 280.0796, found 280.0803). As a result, the reduction of Raman reporters was terminated within 3 h. Without purification, reduced EB and PEP were directly used for the preparation of **SERS probe 1** and **SERS probe 2**-coated silica bead, respectively.

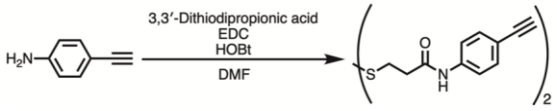

Scheme 1. Synthesis of EP dimer (3,3'-dithiobis[*N*-(4-ethynylphenyl)propanamide]).

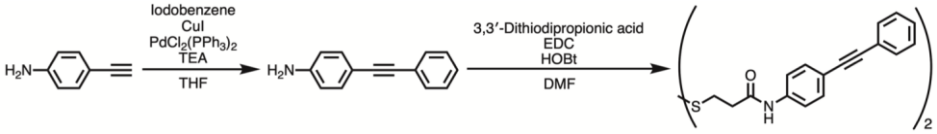

Scheme 2. Synthesis of PEP dimer (3,3'-dithiobis{*N*-[4-(2-phenylethynyl)phenyl]propanamide}).

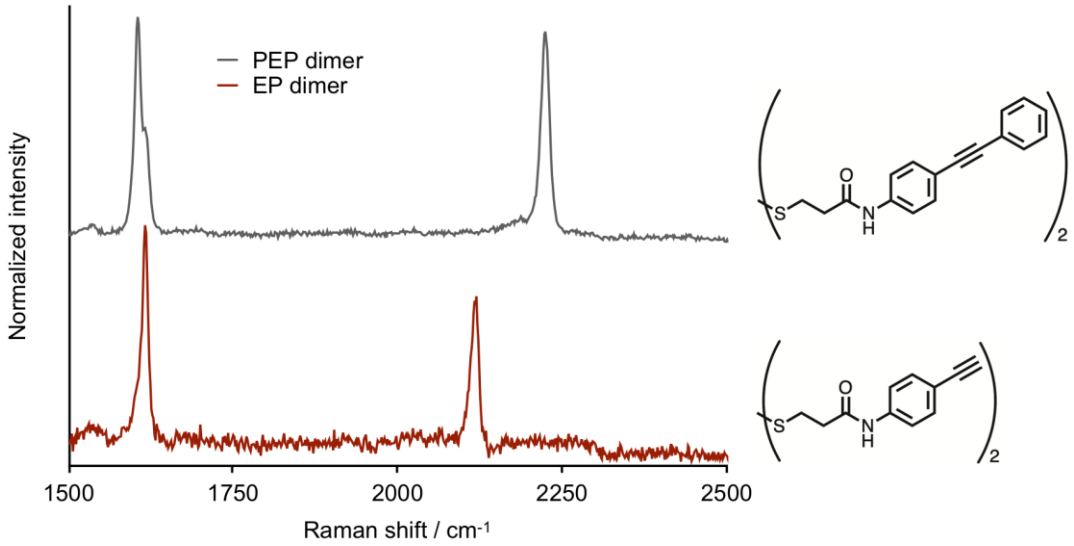

Figure 3. Raman spectra of PEP dimer (gray) and EP dimer (red) with 785 nm of excitation wavelength.

Preparation of **SERS probes 1** were performed as shown in **Scheme 3**. After modifying **5'-HS-DNA** and PEP to the Au-NSs according to our previously reported procedure [26], MCH as a backfill was introduced to the Au-NSs with **5'-HS-DNA** and PEP to improve the colloidal stability of **SERS probe 1** against aggregation and adsorption to amino-modified silica beads. Preparation of **SERS probe 2**-coated silica beads were performed as shown in **Scheme 4**. After immobilizing Au-NSs on the amino-modified silica beads [40], the Au-NS–coated silica beads were functionalized with **3'-HS-DNA** and EP. The optical properties of **SERS probes 1** and **SERS probe 2** were observed by UV-Vis (**Figure 4a**). Note that **SERS probe 2** was isolated from silica beads by sonicating and filtrating **SERS probe 2**-coated silica beads. The LSPR absorbance peaks of **SERS probes 1** and **SERS probe 2** were red-shifted from 775 nm to 805 nm and 810 nm, respectively, because of an increase in the local refractive index at the Au-NS by modifying thiolated DNAs, Raman reporters, and MCH [41]. The amounts of thiolated DNAs modified on the SERS probes were estimated according to Mirkin's procedure [42]. SERS probes and SERS probe-coated silica beads with **HS-DNA-F**, which is a 25-mer DNA with a mercapto group at the 5' end and fluorescein at the 3' end, were prepared according to the same procedure for the preparation of SERS probes. In the case of SERS probe-coated silica beads, SERS probes with **HS-DNA-F** were first separated from silica beads by sonicating and filtrating. Then, the introduced **HS-DNA-F** was liberated from the Au-NS by adding an excess of mercaptoethanol and isolated from the Au-NSs by centrifuging. The average number of loaded **HS-DNA-F** on an Au-NS was estimated from the fluorescence intensity of the supernatants (**Figure 4b**), resulting in the average number of immobilized thiolated DNA of 1420 ± 70 and 1700 ± 130 strands per particle on the **SERS probes 1** and **SERS probe 2**, respectively. The introduction of Raman reporters onto the SERS probes was confirmed by Raman measurement (**Figure 4c**). The Raman spectra of **SERS probes 1** and **SERS probe 2** had SERS signals derived from PEP (1604.92 cm^{-1} (νPh), 1616.10 cm^{-1} (νPh), 2224.19 cm^{-1} (νC≡C)) and EP (1616.10 cm^{-1} (νPh), 2116.57 cm^{-1} (νC≡C)), respectively. These results indicate that Au-NSs were modified with Raman reporters. Moreover, because these SERS signals derived from the ethynyl group of EP and PEP were completely separated, these molecules were good bioorthogonal Raman reporters for the ratiometric SERS assay.

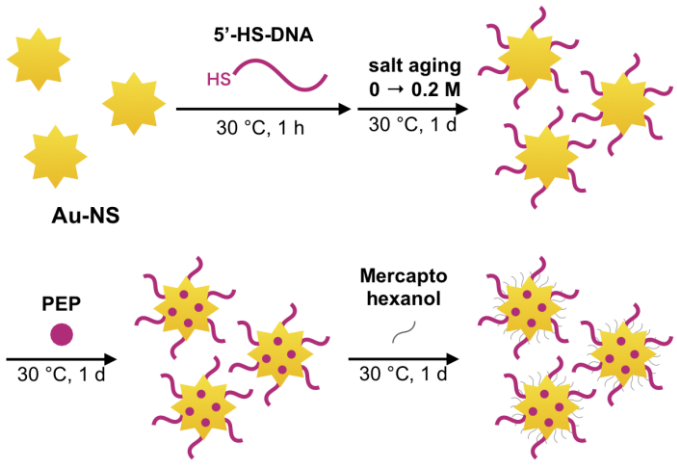

Scheme 3. Procedures for preparation of **SERS probe 1**.

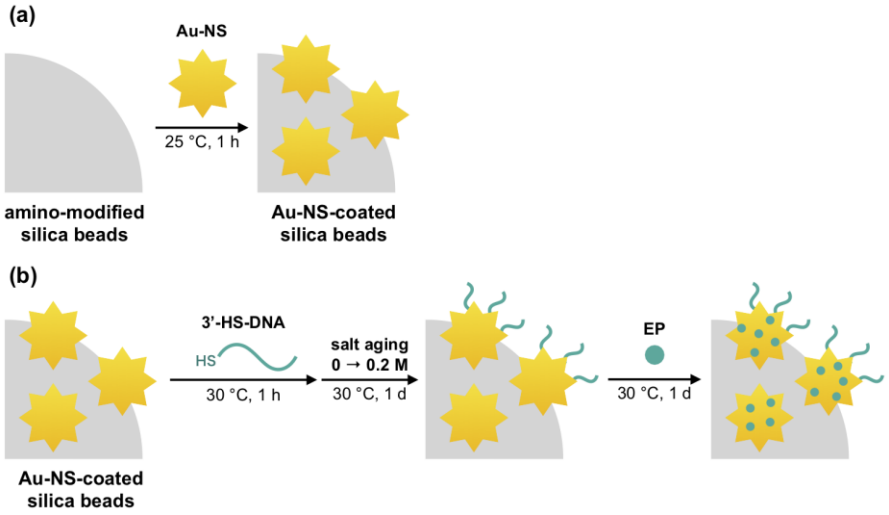

Scheme 4. Procedures for preparation of (a) Au-NS-coated silica beads and (b) **SERS probe 2**-coated silica bead.

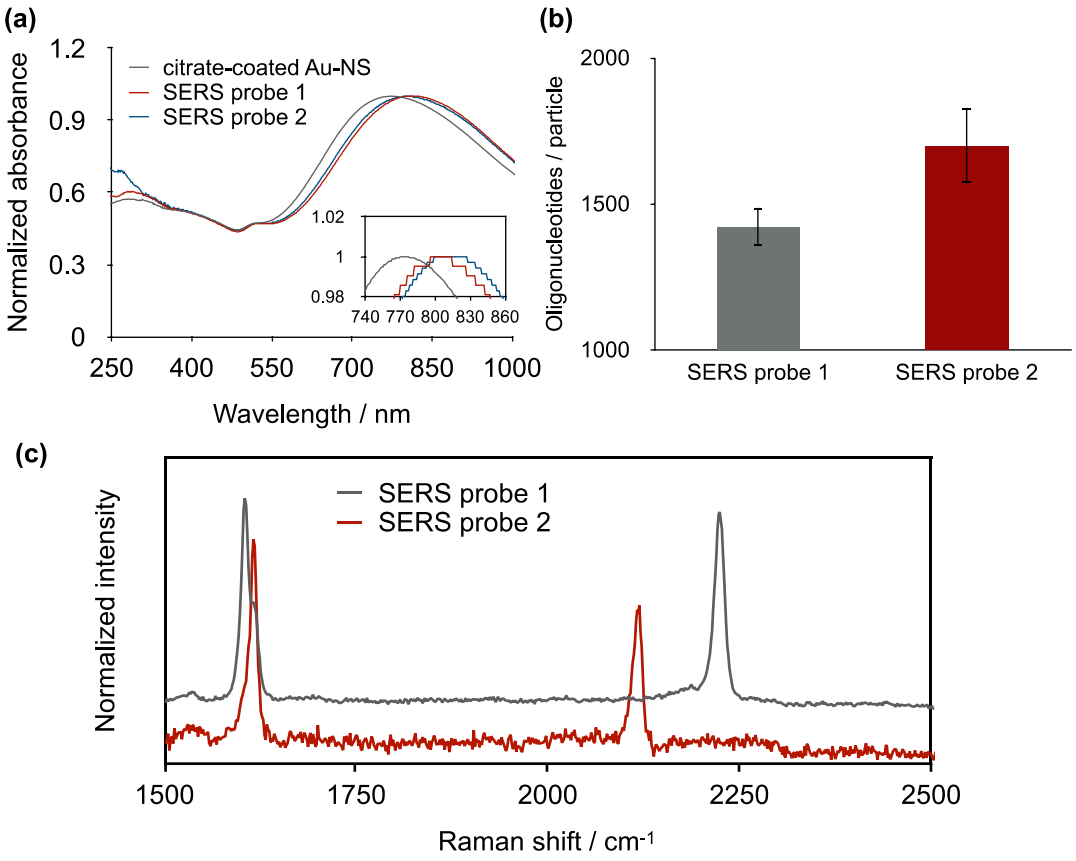

Figure 4. (a) UV-Vis spectra of citrate-coated Au-NSs (gray), **SERS probe 1** (red), and **SERS probe 2** (blue). The inset shows a zoom for a wavelength between 740 and 860 nm. (b) Number of loaded thiolated DNAs on **SERS probe 1** (gray bar) and **SERS probe 2** (red bar). The error bars indicate the standard deviations calculated from two measurements. (c) Raman spectra of **SERS probe 1** (gray) and **SERS probe 2** (red) with 785 nm excitation wavelength.

To determine the sensitivity of ratiometric SERS assay using the SERS probes, **SERS probe 1** and **SERS probe 2**-coated silica bead were mixed with concentrations of **cDNA** ranging from 0 M to 1 nM (**Figure 5**). The Raman spectra of the ratiometric SERS assay were obtained by measuring the regions where the concentrated SERS probes were present (**Figure 5a**), resulting in the clear observation of the SERS signals derived from EP (2117 cm^{-1}) and PEP (2224 cm^{-1}). From these Raman spectra, the RPA (relative peak area) of the SERS signal of PEP were calculated by normalizing the PA (peak area) of PEP by that of EP (**Figure 5b**). The ratiometric SERS assay detected an increase in the RPA as a function of different concentration of **cDNA**. This assay showed a good linear response to the **cDNA** concentration in the range between 0 and 1 nM (R^2=0.98). Without normalization by internal standard, the increase in the PA showed weak association with the concentration of **cDNA**s compared with that in the RPA (R^2=0.83). Note that the standard deviations of PA were comparable to those of RPA since obtained Raman spectra with clear SERS signals derived from EP and PEP were used for peak estimation. The ratiometric SERS assay determined a detection limit of 86 pM. These results suggest that the normalization of the SERS signal by internal standard allows for a decrease in the RSD (relative standard deviation) values of PA of SERS signals and the improvement in the accuracy of SERS-based assays.

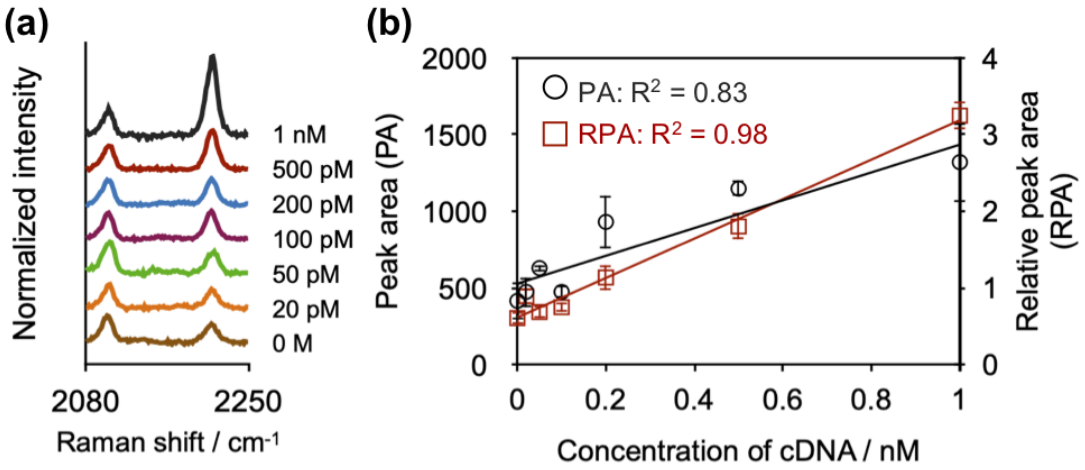

Figure 5. Sensitivity of ratiometric SERS assay using **SERS probe 1** and **SERS probe 2**-coated silica beads for quantification of **cDNA**. (a) Raman spectra of ratiometric SERS assay with different concentrations of **cDNA** (0 to 1 nM). (b) PA (black circle) and RPA (red cube) of PEP as functions of the different concentrations of **cDNA**. The error bars indicate the standard deviations calculated from five measurements. PA: peak area, RPA: relative peak area.

Sequence selectivity is an important figure of merit for nucleic acid detection methods. To evaluate the sequence selectivity of ratiometric SERS assay using **SERS probe 1** and **SERS probe 2**-coated silica bead, I performed ratiometric SERS assay in the presence of **cDNA** or **rDNA** (a 30-mer DNA with a random sequence) (**Figure 6**). In the presence of **cDNA**, the RPA of PEP was remarkably increased compared with that in the presence of **rDNA** and the absence of DNA. These results show that the ratiometric SERS assay enables us to accurately discriminate between target sequences and random sequences.

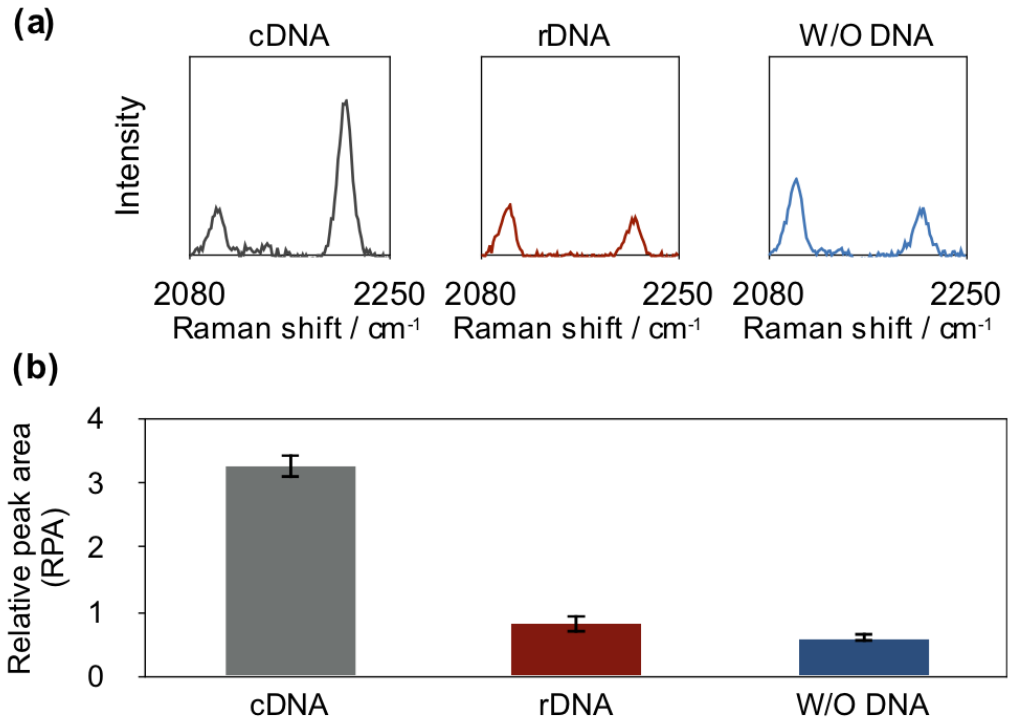

Figure 6. Sequence selectivity of ratiometric SERS assay using **SERS probes 1** and **SERS probe 2**-coated silica beads for quantifying **cDNA**. (a) Raman spectra of ratiometric SERS assay in the presence of **cDNA** and **rDNA** and the absence of DNA. (b) RPA of PEP in the presence of **cDNA** (gray bar) and **rDNA** (red bar) and the absence of DNA (blue bar). The error bars indicate the standard deviations calculated from five measurements. RPA: relative peak area.

In order to realize an automated ratiometric SERS assay with appropriate standard deviations and reproducibility, it is necessary to automatically discriminate spots suitable for laser irradiation, which are selected by highly trained technical experts. To further demonstrate the automatic measurement and analysis of Raman spectra of the ratiometric SERS assay, SERS mapping analysis was carried out in the presence of 500 pM **cDNA** (**Figure 7**). The microscopic image shows the region (20 × 18 μm^2) measured by the SERS mapping analysis, and the dark region indicates concentrated SERS probes. Although the increases in SERS signals of EP and PEP were observed only in the dark region of the microscopic image (**Figure 7a,b**), there were variations in the intensities of SERS signals depending on the measurement location. Measurement spots with the value of PA of EP more than a threshold value (EP $\geq$ 100) were automatically selected by screening process. Then, Raman spectra at selected measurement spots were automatically processed by normalization process of SERS intensities. Without the screening and normalization process, the RSD of PA was 112%, while the RSD of RPA was dramatically improved to 24% by the screening and normalization process (**Figure 7c**). The **cDNA** concentration was estimated from the value of RPA by the calibration curve (**Figure 5b**, red line), resulting in that of 560 pM, which generally corresponded with the prepared concentration (500 pM). These results indicate that the ratiometric SERS assay is a feasible approach for automatically quantifying **cDNA**.

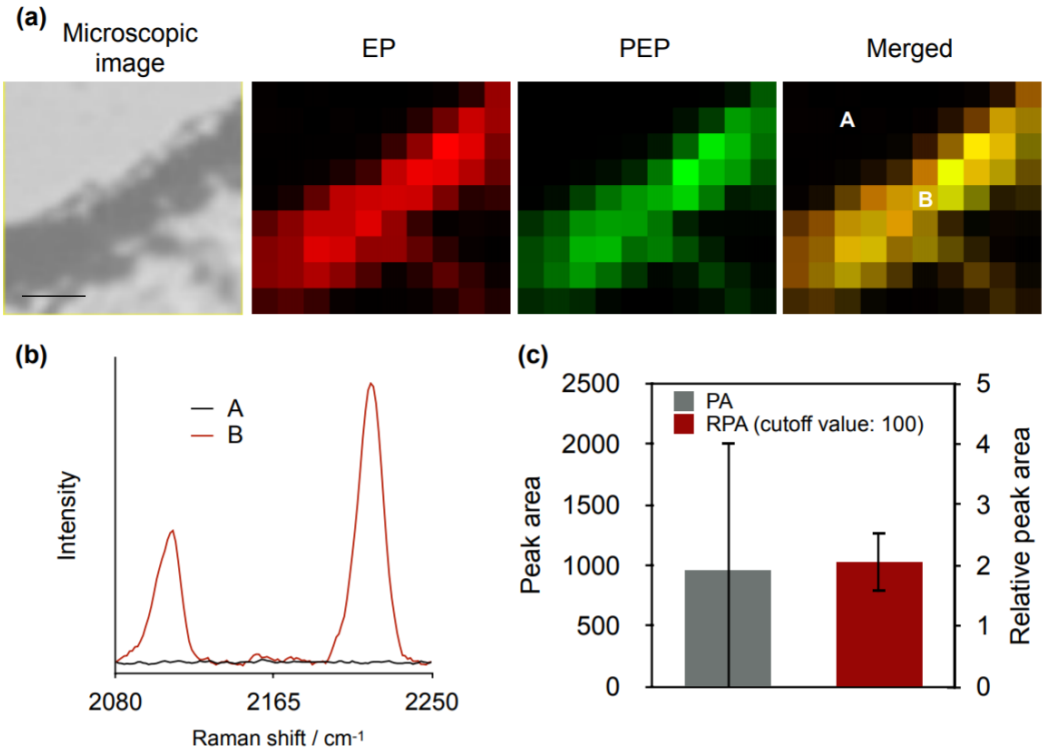

Figure 7. Automated assay for detecting **cDNA** by ratiometric SERS assay. (a) Microscopic and SERS mapping images of dried SERS probes obtained from the ratiometric SERS assay in the presence of 500 pM **cDNA**. EP and PEP represent SERS mapping images plotting the PAs of EP and PEP, respectively. Scale bar: 5 μm. Measurement area: 20 × 18 μm^2, Number of spots: 90. (b) Raman spectra obtained from SERS mapping images at spot A (gray) and spot B (red). (c) The PA (gray bar) and RPA (red bar) of PEP calculated from automatic analysis of SERS mapping. PA and RPA represent the average PA of PEP collected from 90 spectra and the average RPA of PEP collected from 55 spectra with the PA of EP larger than 100. PA: peak area, RPA: relative peak area, RSD: relative standard deviation.

Conclusion

In this chapter, I developed a novel ratiometric SERS assay for quantifying target DNAs by using **SERS probe 1** and **SERS probe 2**-coated silica bead. 86 pM **cDNA**s were successfully detected by the ratiometric SERS assay without amplification process of nucleic acids. Application of the ratiometric SERS assay to automatic detection of target DNAs indicated that SERS-based quantification methods with internal standard were a promising approach for accurate, facile, and sensitive quantification of various biomarkers, such as nucleic acids, metabolites, and proteins.

Materials and methods

Materials and Reagents. Reagents and solvents were purchased from commercial sources. NMR spectra were recorded on a 300 MHz NMR spectrometer (Bruker: AVANCE II 300). Disulfide-modified DNAs were synthesized on an automated DNA synthesizer, and thiolated DNAs were purified using gel filtration chromatography packed with Sephadex (NAP-5 columns). A target DNA and random DNA were purchased from commercial sources. A TEM (JEOL: JEM-2100) was used to measure the diameter and shape of silver seeds and gold nanostars (Au-NSs). The concentration of gold and silver ions was estimated by the ICP-OES (AMETK: SPECTRO BLUE). The ESI-TOF MS (Bruker: micro TOF LC) was used to monitor the reduction reaction of a disulfide bond. A UV-Vis spectrometer (Shimadzu: UV-1800) was used to evaluate the concentrations of DNAs, silver seeds, and Au-NSs. A fluorescence spectrometer (Shimadzu: RF-5300PC) was used to estimate the concentrations of fluorescein-modified DNAs. All Raman measurements were carried out by a micro-Raman spectroscope (Nanophoton: RAMAN-11). A DISMIC-filter (03CP045AN, pore size: 0.45 μm) was used to fractionate the Au-NSs and silica beads (d=1.5 μm).

Synthesis of 3,3'-dithiobis[*N*-(4-ethynylphenyl)propanamide] (EP dimer). 4-Ethynylaniline (59.5 mg, 0.51 mmol) was added to the mixture of 3,3′-dithiodipropionic acid (39.9 mg, 0.19 mmol), EDC hydrochloride (114.8 mg, 0.60 mmol), and HOBt (93.5 mg, 0.61 mmol) in dry DMF (2 mL) and stirred at r.t. overnight. The reaction mixture was quenched by adding saturated sodium hydrogen carbonate and extracted with EtOAc. The extract was washed with saturated sodium hydrogen carbonate and 1 M hydrochloric acid, dehydrated with sodium sulfate, and evaporated under reduced pressure. The residue was purified by flash column chromatography using a gradient elution of (Hexane:EtOAc;90:10 to 50:50), yielding EP dimer (42.3 mg, 0.10 mmol, 55%).
^{1}H NMR (300 MHz, DMSO-d_6) δ10.19 (s, 2H), 7.60 (d, J = 8.7, 4H), 7.40 (d, J = 8.7, 4H), 4.07 (s, 2H), 3.01 (t, J = 6.9, 4H), 2.76 (t, J = 6.9, 4H);
^{13}C NMR (75 MHz, $CDCl_3$) δ169.33, 139.55, 132.32, 118.85, 116.01, 83.52, 79.75, 36.01, 33.29;
HRMS (ESI-TOF) *m/z*: $[M+Na]^+$ calcd for $C_{22}H_{20}N_2O_2S_2Na$ 431.0858; found 431.0880.

Synthesis of 4-(2-phenylethynyl)benzamine. 4-(2-phenylethynyl)benzamine was synthesized following a reported method [43]. 4-Ethynylaniline (118.5 mg, 1.0 mmol), iodobenzene (225 μL, 2.0 mmol) and TEA (2 mL, 14 mol) were dissolved in THF (8 mL) and degassed the solvents by freeze-pump-thaw. Bis(triphenylphosphine)-palladium(II) dichloride (71.8 mg, 0.1 mmol) and copper(I) iodide (22.6 mg, 0.1 mmol) were added to the solvent and stirred at r.t. overnight. The reaction mixture

was extracted with CH_2Cl_2. The extract was washed with water, dehydrated with sodium sulfate, and evaporated under reduced pressure. The residue was purified by flash column chromatography using a gradient elution of (Hexane:EtOAc;90:10 to 30:70), yielding 4-(2-phenylethynyl)benzamine (76.1 mg, 0.39 mmol, 39%).

^{1}H NMR (300 MHz, $CDCl_3$) δ7.49 (d, J = 7.5, 2H), 7.33 (t, J = 7.2, 5H), 6.64 (d, J = 7.5, 2H), 3.81 (s, 2H);

HRMS (ESI-TOF) *m/z*: $[M+Na]^+$ calcd for $C_{14}H_{11}NNa$ 216.0789; found 216.0730.

Synthesis of 3,3'-dithiobis{*N*-[4-(2-phenylethynyl)phenyl]propanamide} (PEP dimer). 4-(2-Phenylethynyl)benzamine (48.5 mg, 0.25 mmol) was added to the mixture of 3,3′-dithiodipropionic acid (20.9 mg, 0.10 mmol), EDC hydrochloride (47.7 mg, 0.25 mmol), and HOBt (38.9 mg, 0.25 mmol) in dry DMF (1 mL). After stirring at r.t. for 16 h, EDC hydrochloride (18.9 mg, 0.10 mmol) and DMAP (25.0 mg, 0.20 mmol) was added to the mixture and stirred for 5 h at r.t.. The reaction mixture was quenched by adding saturated sodium hydrogen carbonate and extracted with EtOAc. The extract was washed with saturated sodium hydrogen carbonate and 1 N hydrochloric acid, dehydrated with sodium sulfate, and evaporated under reduced pressure. The residue was purified by flash column chromatography using a gradient elution of (Hexane:EtOAc;50:50 to 0:100), yielding PEP dimer (49.5 mg, 0.09 mmol, 88%).

^{1}H NMR (300 MHz, DMSO-d_6) δ10.23 (s, 2H), 7.65 (d, J = 8.1, 4H), 7.52 (m, 8H), 7.41 (d, J = 4.5, 6H), 3.04 (t, J = 6.6, 4H), 2.78 (t, J = 6.9, 4H);

^{13}C NMR (75 MHz, $CDCl_3$) δ169.35, 139.46, 132.03, 131.19, 128.69, 128.51, 122.49, 118.94, 116.50, 89.47, 88.47, 36.04, 33.35;

HRMS (ESI-TOF) *m/z*: $[M–H]^-$ calcd for $C_{34}H_{27}N_2O_2S_2$ 559.1592; found 559.1642.

Synthesis of silver seeds and citrate capped Au-NSs. Screw cap bottles and stir bars were treated with aqua regia before synthesis of silver seeds and Au-NSs. Silver seeds were synthesized by previously reported [37]. Trisodium citrate (5 mM, 250 μL) was added to the solution of $AgNO_3$ (250 μM, 10 mL). After stirring for 1 min, $NaBH_4$ (40 mM, 400 μL), which was freshly prepared and cooled in the refrigerator for 15 min, was added to the reaction mixture and stirred at r.t. without closing the cap. After 5 min, the stir bar was removed from the screw cap bottle. The reaction mixture was kept in dark place for 2 h without closing the cap, yielding silver seeds. Gold nanostars were prepared according to a previous report [38]. The synthesized silver seeds (200 μL) were added to Milli-Q water (19.8 mL) and stirred at r.t.. Then, chloroauric acid tetrahydrate (25 mM, 200 μL) was added to the solution. After stirring for 15 s, silver nitrate (2.5 mM, 80 μL) and ascorbic acid (freshly prepared, 100 mM, 100 μL) were concomitantly added to the reaction mixture and stirred at r.t. for 5 min, yielding naked Au-NSs. To inhibit aggregation of the Au-NSs, poly(styrenesulfonate) (PSS) (18%, 171 μL)

was added to the Au-NSs dispersion immediately and stirred at r.t. for 2 h. PSS-coated Au-NSs were converted into citrate-coated Au-NSs as previously reported [39]. The PSS-capped Au-NSs dispersion (5 mL) was centrifuged at 3,000 rpm for 20 min in 15-mL plastic tubes. The supernatant was removed until 1 mL of the retentate, and the Au-NSs were redispersed into 5 mL of 5 mM trisodium citrate. The Au-NSs were subjected to four cycles of centrifugation, removal of supernatant, and redispersion (C/R/R) in the same manner and stood at r.t. for 1 day. Additionally, the Au-NSs were subjected to four C/R/R cycle, yielding citrate-capped Au-NSs dispersion in 5 mM trisodium citrate.

Estimation of extinction coefficient of silver seeds and Au-NSs. Silver seeds (2.5 OD) or Au-NSs (2.0 OD) suspension (200 μL) were added to aqua regia (400 μL) to dissolve the metal nanoparticles. The solutions were diluted by Milli-Q water to 3% aqua regia and monitored by the ICP-OES. Concentrations of gold and silver ions were determined from the calibration curves of gold and silver ions, which were obtained with a range of 0–10 ppm of $HAuCl_4$ in 3% HCl and $AgNO_3$ in 3% HNO_3, respectively. Extinction coefficient of Au-NSs and silver seeds were calculated from the concentration of metallic ions, the absorption, and the diameter and shape of metallic nanoparticles estimated from TEM images.

Preparation of Au-NS-coated silica beads. Au-NS-coated silica beads were prepared following to a previous report [40]. To adsorb the Au-NSs onto amino-modified silica beads, Au-NSs (2.8 fmol) were added to the amino-modified silica beads (500 μg) in 250 μL of 10 mM phosphate buffer (pH7.0) containing 0.05% SDS and stirred at 25 °C for 1 h. To remove excess Au-NSs, the silica beads were centrifuged and the supernatant was removed, leaving a pellet of Au-NSs-coated silica beads at the bottom.

Preparation of SERS probe 1 and SERS probe 2-coated silica bead. SERS probe 1 and **SERS probe 2**-coated silica beads were prepared as follows:

1. **Introduction of thiolated oligonucleotides onto Au-NSs and Au-NS-coated silica beads.** Since thiolated-oligonucletides tends to form disulfide bond for protection of thiol groups, the disulfide bond of the oligonucleotides were cleaved by reduction with tris(2-carboxyethyl)phosphine hydrochloride (TCEP-HCl) before use. Disulfide-modified oligonucleotides (5.0 nmol) and TCEP-HCl (1.0 μmol) were dissolved in sterile water (100 μL) and incubated at 30 °C for 3 h. The reaction mixture was purified by NAP-5 columns. The purified oligonucleotides were analyzed by ESI-TOF-MS spectrometry. HRMS (ESI-TOF-MS) m/z: $[M–5H]^{5-}$ calcd for **5'-HS-DNA-F** 1690.49, found 1690.58; $[M–5H]^{5-}$ calcd for **5'-HS-DNA** 1576.67, found 1576.64. $[M–5H]^{5-}$ calcd for **3'-HS-DNA** 1544.86, found 1544.82. The purified oligonucleotides (250 pmol) were added to the solution of Au-NSs (2.8 fmol) or Au-NS-coated silica beads (500 μg) in 250 μL

of 10 mM phosphate buffer (pH7.0) containing 0.05% SDS and stirred at 30 °C for 1 h. Then, to reduce electrostatic repulsions of the negative charge of oligonucleotides, the concentration of NaCl was increased to 200 mM by salt aging processes. 4 M NaCl was gradually added to the reaction mixture (up to 100 mM of NaCl; 50 mM NaCl increments / 30 min, up to 200 mM of NaCl; 100 mM increments / 30 min) until 200 mM NaCl concentration followed by stirring at 30 °C overnight. To remove the excess oligonucleotides, the reaction mixture was centrifuged (Au-NSs: at 3,000 rpm for 5 min, Au-NS-coated silica beads: at 6,000 rpm for 5 s) and the supernatant was removed to a final volume of 50 μL. The pellet was resuspended in 250 μL of 10 mM phosphate buffer containing 0.05% SDS. The Au-NSs and Au-NS-coated silica beads were subjected to three cycles of centrifugation, removal of supernatant, and redispersion. Lastly, the Au-NS and Au-NS-coated silica bead dispersions were enriched to a final volume of 50 μL by removal of the supernatant after centrifugation.

2. **Introduction of Raman reporters onto Au-NSs and Au-NS-coated silica beads with thiolated DNAs.** To obtain the Raman reporters (PEP or EP), Raman reporter dimers (5.0 nmol) and TCEP-HCl (1.0 μmol) were dissolved in *N*,*N*-dimethylformamide (90 μL) and sterile water (10 μL). The reaction mixture was incubated at 30 ºC for 3 h. The product of the reduction reaction was analyzed by ESI-TOF-MS spectrometry. HRMS (ESI-TOF-MS) *m*/*z*: $[M–H]^-$ calcd for $C_{10}H_9N_2OS$ (EP) 204.0483, found 204.0495, $[M–H]^-$ calcd for $C_{10}H_9N_2OS$ (PEP) 280.0796, found 280.0803. PEP (250 pmol) and EP (250 pmol) were added to Au-NSs (2.8 fmol) with **5'-HS-DNA** and Au-NS-coated silica beads (500 μg) with **3'-HS-DNA**, respectively, in 250 μL of 10 mM phosphate buffer (pH7.0) containing 0.05% SDS and stirred at 30 °C overnight. Removal of excess of Raman reporters was performed according to the same procedure as removal of excess oligonucleotides. Prepared **5'-HS-DNA**- and PEP-co-modified Au-NSs were used on the introduction of mercaptohexanol. Au-NS-coated silica beads with **3'-HS-DNA** and EP were named **SERS probe 2**-coated silica beads.

3. **Introduction of mercaptohexanol onto Au-NSs.** Au-NSs (2.8 fmol) with **5'-HS-DNA** and PEP were added to the solution of MCH (250 pmol) in 250 μL of 10 mM phosphate buffer (pH7.0) containing 0.05% SDS and stirred at 30 °C overnight. Removal of excess of MCH was performed according to the same procedure as removal of excess oligonucleotides. Prepared **5'-HS-DNA-**, PEP-, and MCH-co-modified Au-NSs were named **SERS probe 1**.

Estimation of the amount of Au-NSs immobilized onto silica beads. SERS probe 2-coated silica beads (500 μg) were added in 100 μL of 10 mM phosphate buffer (pH7.0) containing 0.05% SDS, sonicated for 20 sec, and filtrated. The solution was monitored by UV-Vis spectrometer.

Quantification of the number of oligonucleotides on SERS probe 1 and 2. SERS probe 1 and **SERS probe 2**-coated silica bead with **5'-HS-DNA-F** were prepared according to preparation of **SERS probe 1** and **SERS probe 2**-coated silica bead. To obtain **SERS probe 2**, **SERS probe 2**-coated silica beads (500 μg) with **5'-HS-DNA-F** were sonicated for 20 sec and filtrated. **SERS probe 1** (1.5 fmol) and **SERS probe 2** (estimated value: 0.5 fmol) with **5'-HS-DNA-F** were added to mercaptohexanol (3.2 μmol) in 270 μL of 10 mM phosphate buffer containing 0.05% SDS and 0.3 M NaCl at 30 ºC for 1 day. After incubation, the reaction mixtures were centrifuged at 3,000 rpm for 5 min and the supernatants were recovered. The dissociated **5'-HS-DNA-F** was monitored by the fluorescence spectrometer. Concentration of dissociated **5'-HS-DNA-F** in the supernatants was calculated using the fluorescence intensity at 520 nm. The number of **5'-HS-DNA-F** on a Au-NS was estimated from the concentration of dissociated **5'-HS-DNA-F** and Au-NSs.

Detection of cDNA by ratiometric SERS assays. The DNAs (**cDNA** or **rDNA**) were added to the solution of **SERS probe 1** (1.0 fmol) and **SERS probe 2**-coated silica bead (400 μg) in 100 μL of 10 mM phosphate buffer (pH7.0) containing 0.05% SDS and 0.3 M NaCl and stirred at 25 °C for 6 h. After mixing, the reaction mixture was filtrated to separate the **SERS probe 1**–**SERS probe 2**-coated silica bead complexes from surplus **SERS probe 1**. The fractionated complexes were washed with 100 μL of 10 mM phosphate buffer (pH7.0) containing 0.3 M NaCl and 0.05% SDS and recovered with 50 μL of 10 mM phosphate buffer (pH7.0) containing 0.05% SDS. The complexes were sonicated for 20 sec to liberate the Au-NSs from the silica beads and filtrated to remove the silica beads. The solution was centrifuged at 3,000 rpm for 5 min and removed 40 μL of the supernatant to concentrate the SERS probes. The concentrated SERS probes (1.5 μL) were dried on the glass slide and measured by micro-Raman spectroscopy (Conditions; Laser: 785 nm, Grating: 300 mm^{-1}, Exposure time: 10 s, Laser power: 47.8 mW, Lens: ×50).

References

[1]. Heilek, G. in *Nucleic Acids — The Use of Nucleic Acid Testing in Molecular Diagnostics, Nucleic Acids - From Basic Aspects to Laboratory Tools*, Larramendy, M. L.; Soloneski, S. IntechOpen, **2016**, 75–91.

[2]. Suraj, S.; Dhar, C.; Srivastava, S. *Biomed. Rep.* **2017**, *6*, 8–14.

[3]. Chen, C.; Ridzon, D. A.; Broomer, A. J.; Zhou, Z.; Lee, D. H.; Nguyen, J. T.; Barbisin, M.; Xu, N. L.; Mahuvakar, V. R.; Andersen, M. R.; Lao, K. Q.; Livak, K. J.; Guebler, K. J. *Nucleic Acids Res*. **2005**, *33*, e179.

[4]. Fleischmann, M.; Hendra, P. J.; McQuillan, A. J. *J. Chem. Phys. Lett.* **1974**, *26*, 163–166.

[5]. Campion, A.; Patanjali, K. *Chem. Soc. Rev*. **1998**, *27*, 241–250.

[6]. Wang, Y.; Yan, B.; Chen, L. *Chem. Rev.* **2013**, *113*, 1391–1428.

[7]. Qi, G.; Jia, K.; Fu, C.; Xu, S.; Xu, W. *J. Opt.* **2015**, *17*, 114020.

[8]. Tang, L.; Li, S.; Han, F.; Liu, L.; Xu, L.; Ma, W.; Kuang, H.: Li, A.; Xu, C. *Biosens. Bioelectron.* **2015**, *71*, 7–12.

[9]. Wang, Z.; Yang, H.; Wang, M.; Petti, L.; Jiang, T.; Jia, Z.; Xie, S.; Zhou, J. *Colloids Surf. A Physicochem. Eng. Asp.* **2018**, *546*, 48–58.

[10]. Chang, H.; Kang, H.; Ko, E.; Jun, B. H.; Lee, H. Y.; Jeong, D. H. *ACS Sens.* **2016**, *1*, 645–649.

[11]. Yang, Y.; Jiang, X.; Chao, J.; Song, C.; Liu, B.; Zhu, D.; Sun, Y.; Yang, B.; Zhang, Q.; Chen, Y.; Wang, L. *Sci. China Mater.* **2017**, *60*, 1129–1144.

[12]. Qian, Y.; Fan, T.; Yao, Y.; Shi, X.; Liao, X.; Zhou, F.; Gao, F. *Sens. Actuators B Chem.* **2018**, *254*, 483–489.

[13]. Ye, S.; Wu, Y.; Zhai, X.; Tang, B. *Anal. Chem.* **2015**, *87*, 8242–8249.

[14]. Shi, H.; Chen, N.; Su, Y.; Wang, H.; He, Y. *Anal. Chem.* **2017**, *89*, 10279–10285.

[15]. Wu, Y.; Xiao, F.; Wu, Z.; Yu, R. *Anal. Chem.* **2017**, *89*, 2852–2858.

[16]. Wang, H.; Jiang, X.; He, Y. *Analyst* **2016**, *141*, 5010–5019.

[17]. Bell, S. E. J.; Sirimuthu, N. M. S. *Chem. Soc. Rev.* **2008**, *37*, 1012–1024.

[18]. Schluker, S. *Angew. Chen. Int. Ed.* **2014**, *53*, 4756–4795.

[19]. Shen, W.; Lin, X.; Jiang, C.; Li, C.; Lin, H.; Huang, J.; Wang, S.; Liu, G.; Yan, X.; Zhong, Q.; Ren, B. *Angew. Chem. Int. Ed.* **2015**, *54*, 7308–7312.

[20]. Xu, L. J.; Lei, Z. C.; Li, J.; Zong, C.; Yang, C. J.; Ren, B. *J. Am. Chem. Soc.* **2015**, *137*, 5149–5154.

[21]. Zhang, Y.; Zou, Y.; Liu, F. Xu, Y.; Wang, X.; Li, Y.; Liang, H.; Chen, L.; Chen, Z.; Tan, W. *Anal. Chem.* **2016**, *88*, 10611–10616.

[22]. Wu, Y.; Jiang, T.; Wu, Z.; Yu, R. *Talanta* **2018**, *185*, 30–36.

[23]. Chen, J.; Wu, Y.; Fu, C.; Cao, H.; Tan, X.; Shi, W.; Wu, Z. *Biosens. Bioelectron.* **2019**, *143*, 111619.

[24]. Yamakoshi, H.; Dodo, K.; Okada, M.; Ando, J.; Palonpon, A.; Fujita, K.; Kawata, S.; Sodeoka, M. *J. Am. Chem. Soc.* **2011**, *133*, 6102–6105.

[25]. Qin, X.; Lyu, M.; Si, Y.; Yang, J.; Wu, Z.; Li, J. *Anal. Chim. Acta* **2018**, *1043*, 115–122.

[26]. Ota, R.; Takagi, N.; Imaizumi, Y.; Waku, T.; Kobori, A. *Nucleosides Nucleotides Nucleic Acids* **2020**, in press.

[27]. Swager, T. M.; Weizmann, Y.; Chenoweth, D. M. U.S. Pat. Appl. Publ. US 2011/0171629 A1, **2010**.

[28]. Li, M.; Cushing, S. K.; Zhang, J.; Lankford, J.; Aguilar, Z. P.; Ma, D.; Wu, N. *Nanotechnology* **2012**, *23*. 115501.

[29]. Yuan, H.; Fales, A. M.; Khoury, C. G.; Liu, J.; Vo-Dinh, T. *J. Raman Spectrosc*. **2013**, *44*, 234–239.

[30]. Pei, Y.; Wang, Z.; Zong, S.; Cui, Y. *J. Mater. Chem. B* **2013**, *1*, 3992–3998.

[31]. Zheng, P.; Li, M.; Jurevic, R.; Cushing, S. K.; Liu, Y.; Wu, N. *Nanoscale* **2015**, *7*, 11005–11012.

[32]. Li, A.; Tang, L.; Song, D.; Song, S.; Ma, W.; Xu, L.; Kuang, H.; Wu, X.; Liu, L.; Chen, X.; Xu, C. *Nanoscale* **2016**, *8*, 1873–1878.

[33]. Ma, W.; Sun, M.; Xu, L.; Wang, L.; Kuang, H.; Xu, C. *Chem. Commun.* **2013**, *49*, 4989–4991.

[34]. Trigari, S.; Rindi, A.; Margheri, G.; Sottini, S.; Dellepiane, G.; Giorgetti, E. *J. Mater. Chem.* **2011**, *21*, 6531–6540.

[35]. Kedia, A.; Kumar, P. S. *J. Mater. Chem. C* **2013**, *1*, 4540–4549.

[36]. He, S. Kang, M. W. C.; Khan, F. J.; Tan, E. K. M.; Reyes, M. A.; Kah, J. C. Y. *J. Opt.* **2015**, *17*, 114013.

[37]. Kereselidze, Z.; Romero, V. H.; Peralta, X. G.; Santamaria, F. *J. Vis. Exp.* **2012**, *59*, e3570.

[38]. Lee, Y. J.; Ahn, E. Y.; Park, Y. *Nanoscale Research Letters* **2019**, *14*, 129.

[39]. Mehtala, J. G.; Zemlyanov, D. Y.; Max, J. P.; Kadasaka, N.; Zhao, S.; Wei, A. *Langmuir* **2014**, *30*, 13727–13730.

[40]. Serrano-Montes, A. B.; Langer, J.; Henriksen-Lacey, M.; Jimenez De Aberasturi, D.; Solís, D. M.; Taboada, J. M.; Obelleiro, F.; Sentosun, K.; Bals, S.; Bekdemir, A.; Stellacci, F.; Liz-Marzán, L. M. *J. Phys. Chem. C* **2016**, *120*, 20860–20868.

[41]. Xie, J.; Zhang, Q.; Lee, J. Y.; Wang, D. I. C. *ACS Nano* **2008**, *2*, 2473–2480.

[42]. Demers, L. M.; Mirkin, C. A.; Mucic, R. C.; Reynolds, R. A.; Letsinger, R. L.; Elghanian, R.; Viswanadham, G. *Anal. Chem.* **2000**, *72*, 5535–5541.

[43]. Zhao, C. Q.; Chen, Y. G.; Qiu, H.; Wei, L.; Fang, P.; Mei, T. S. *Org. Lett.* **2019**, *21*, 1412–1416.

List of publications

Chapter 1: Ryo Ota, Noriyuki Takagi, Yu Imaizumi, Tomonori Waku, Akio Kobori.
"Sandwich-type detection of nucleic acids by bioorthogonal SERS probes"
Nucleosides, Nucleotides and Nucleic Acids, **2021**, *40*, 166-177.

Chapter 2: Ryo Ota, Yuki Fukushima, Yuta Araki, Kenta Sasaki, Tomonori Waku, Akio Kobori.
"Ratiometric SERS assays for reliable and automatic quantification of nucleic acids"
Chemistry Letters, **2020**, Advance publication, DOI: 10.1246/cl.200798.

Acknowledgements

The study presented in this Doctoral Dissertation was carried out under the direction of Professor **Akio Kobori** at the Faculty of Molecular Chemistry and Engineering, Kyoto Institute of Technology during April 2015 to March 2021. The study is concerned with the SERS-based assays with bioorthogonal Raman reporters for simple and reliable quantification of nucleic acids.

The author wishes to represent my sincere gratitude to Professor Kobori for giving me opportunity to study under his group, furthermore for giving me the encouragement to study, the worthy discussion and the criticism with accuracy. The author is indebted to Assistant professor **Tomonori Waku** at the Faculty of Molecular Chemistry and Engineering, Kyoto Institute of Technology for his helpful advice, discussion and encouragement. The author thanks Professor **Naoto Tsutsumi** at the Faculty of Executive Level, Kyoto Institute of Technology for the microscopic Raman spectrometer and Associate Professor **Hideyuki Nakanishi** at the Faculty of Materials Science and Engineering, Kyoto Institute of Technology for the ICP-OES.

The author thanks great colleagues, Mr. **Yu Watari** and Mr. **Soichi Tatsumi**, for their discussions and encouragement. The authors are very grateful to Mr. **Mitsuhiro Nakamura**, Mr. **Yuki Fukushima**, Mr. **Yuta Araki**, Mr. **Kenta Sasaki**, Mr. **Hidetoshi Nishikawa**, and other colleagues for helpful suggestions and heartful encouragements. I am further thankful to my colleagues, Mr. **Shunsuke Sogo**, Mr. **Shunsuke Ohmura**, and Ms. **Yuki Nagai** for indelible memories we spent together.

To conclude, I further wish to acknowledge the support of **Yumiko Ota** and **Jun Ota**.

Ryo Ota

December, 2020